A simple and accurate algorithm for path integral molecular dynamics with the Langevin thermostat

Cite as: J. Chem. Phys. **145**, 024103 (2016); https://doi.org/10.1063/1.4954990
Submitted: 29 April 2016 . Accepted: 17 June 2016 . Published Online: 11 July 2016

Jian Liu, Dezhang Li, and Xinzijian Liu

A simple and accurate algorithm for path integral molecular dynamics with the Langevin thermostat

Jian Liu,[a] Dezhang Li,[b] and Xinzijian Liu[b]
Beijing National Laboratory for Molecular Sciences, Institute of Theoretical and Computational Chemistry, College of Chemistry and Molecular Engineering, Peking University, Beijing 100871, China

(Received 29 April 2016; accepted 17 June 2016; published online 11 July 2016)

We introduce a novel simple algorithm for thermostatting path integral molecular dynamics (PIMD) with the Langevin equation. The staging transformation of path integral beads is employed for demonstration. The optimum friction coefficients for the staging modes in the free particle limit are used for all systems. In comparison to the path integral Langevin equation thermostat, the new algorithm exploits a different order of splitting for the phase space propagator associated to the Langevin equation. While the error analysis is made for both algorithms, they are also employed in the PIMD simulations of three realistic systems (the H_2O molecule, liquid *para*-hydrogen, and liquid water) for comparison. It is shown that the new thermostat increases the time interval of PIMD by a factor of 4–6 or more for achieving the same accuracy. In addition, the supplementary material shows the error analysis made for the algorithms when the normal-mode transformation of path integral beads is used. *Published by AIP Publishing.* [http://dx.doi.org/10.1063/1.4954990]

I. INTRODUCTION

In 1953, Feynman first presented imaginary time path integral to study liquid helium,[1] which already demonstrated the mapping of a quantum system onto a classical model consisting of the Feynman ring of "beads" (i.e., replicas of the system) connected by harmonic springs.[1] In 1981, Chandler and Wolynes then suggested the quantum-classical isomorphism that established the relationship between quantum concepts and the classical polymer language.[2,3] Imaginary time path integral has not only provided a physical picture but also offered a powerful computational framework for studying quantum statistical effects.[3–5] Such effects (including zero point energy, tunneling, and quantum exchange effects) become important at low temperatures and/or in realistic systems that contain light atoms such as hydrogen or helium.

In 1984, Parrinello and Rahman proposed that artificial momenta could be assigned to the mapping polymer such that molecular dynamics (MD) could be employed to perform the path integral sampling.[6] The normal-mode transformation[7–9] or staging transformation[10,11] was introduced to deal with the stiffness of the harmonic springs between the beads. Thermostatting methods such as the Andersen thermostat,[12] Langevin dynamics,[13,14] and Nosé-Hoover chain (NHC)[10,11] were implemented in path integral molecular dynamics (PIMD) to ensure a proper canonical distribution of the path integral beads. As it is often not a trivial task to adjust moves of path integral Monte Carlo (PIMC) for general molecular systems, path integral molecular dynamics (PIMD) thus offers a more convenient computational technique for simulating structural and thermodynamic properties when quantum exchange effects are not significant.

As early as in 1980s, Langevin dynamics was already introduced for thermostatting PIMD by Gillan[13] and by Singer and Smith.[14] It has also been investigated by Müser[15] and by Drozdov and Talkner.[16] More recently, Ceriotti *et al.* have developed a path integral Langevin equation (PILE) thermostat that combines a simple (white noise) Langevin thermostat with the velocity Verlet algorithm to give an efficient sampling of the canonical distribution for PIMD.[17] It is demonstrated that in terms of sampling efficiency PILE is comparable to the NHC thermostat[10] for PIMD.[17] The implementation of PILE is very straightforward for general molecular systems. These suggest that it is worth investigating more stochastic methods for PIMD.

The purpose of this paper is to present a novel, simple, and accurate algorithm for accomplishing PIMD with Langevin thermostats. Section II first briefly reviews PIMD with the staging transformation of path integral beads. After demonstrating how the PILE thermostat[17] can be implemented for staging PIMD, we introduce a more accurate and robust integrator for propagating PIMD with the (white noise) Langevin thermostat. Section III applies both integrators to three typical realistic molecular systems, namely, the water molecule, liquid *para*-hydrogen, and liquid water. The two integrators are compared by studying two thermodynamic properties: the average kinetic energy (obtained by either the primitive or virial estimator) and the average potential energy. The performance is then investigated as a function of the time interval of PIMD. (More discussions are given in Appendices A-C and in the supplementary material.[18]) Conclusions and outlook follow in Section IV.

II. THEORY

A. Thermodynamic properties

Any thermodynamic property of the canonical ensemble is of the general form

[a]Electronic mail: jianliupku@pku.edu.cn
[b]D. Li and X. Liu contributed equally to this work.

$$\langle \hat{B} \rangle = \frac{1}{Z} \mathrm{Tr}\left(e^{-\beta \hat{H}} \hat{B}\right), \tag{1}$$

where $Z = \mathrm{Tr}\left[e^{-\beta \hat{H}}\right]$ ($\beta = 1/k_B T$) is the partition function, $\hat{H}$ is the (time-independent) Hamiltonian of the system with the total number of degrees of freedom N, which we assume to be of the standard Cartesian form

$$\hat{H} = \frac{1}{2} \hat{\mathbf{p}}^T \mathbf{M}^{-1} \hat{\mathbf{p}} + V(\hat{\mathbf{x}}), \tag{2}$$

where $\mathbf{M}$ is the diagonal "mass matrix" with elements $\{m_j\}$, and $\hat{\mathbf{p}}$ and $\hat{\mathbf{x}}$ are the momentum and coordinate operators, respectively; and $\hat{B}$ is an operator relevant to the specific property of interest.

Express Eq. (1) in the coordinate space $\mathbf{x}$, i.e.,

$$\langle \hat{B} \rangle = \frac{\int d\mathbf{x} \langle \mathbf{x} | e^{-\beta \hat{H}} \hat{B} | \mathbf{x} \rangle}{\int d\mathbf{x} \langle \mathbf{x} | e^{-\beta \hat{H}} | \mathbf{x} \rangle}. \tag{3}$$

Inserting path integral beads to evaluate the term $\langle \mathbf{x} | e^{-\beta \hat{H}} | \mathbf{x} \rangle$ leads to

$$Z = \int d\mathbf{x} \langle \mathbf{x} | e^{-\beta \hat{H}} | \mathbf{x} \rangle \overset{\mathbf{x}_1 \equiv \mathbf{x}}{=} \lim_{P \to \infty} \int d\mathbf{x}_1 \int d\mathbf{x}_2 \cdots \int d\mathbf{x}_P \left(\frac{P}{2\pi\beta\hbar^2}\right)^{NP/2} |\mathbf{M}|^{P/2} \exp\left\{-\frac{P}{2\beta\hbar^2} \sum_{i=1}^{P} \left[(\mathbf{x}_{i+1} - \mathbf{x}_i)^T \mathbf{M} (\mathbf{x}_{i+1} - \mathbf{x}_i)\right] - \frac{\beta}{P} \sum_{i=1}^{P} V(\mathbf{x}_i)\right\}, \tag{4}$$

where $\mathbf{x}_{P+1} \equiv \mathbf{x}_1$ and P is the number of path integral beads. Then the numerator of Eq. (3) becomes

$$\int d\mathbf{x} \langle \mathbf{x} | e^{-\beta \hat{H}} \hat{B} | \mathbf{x} \rangle \overset{\mathbf{x}_1 \equiv \mathbf{x}}{=} \lim_{P \to \infty} \int d\mathbf{x}_1 \int d\mathbf{x}_2 \cdots \int d\mathbf{x}_P \left(\frac{P}{2\pi\beta\hbar^2}\right)^{NP/2} |\mathbf{M}|^{P/2} \times \exp\left\{-\frac{P}{2\beta\hbar^2} \sum_{i=1}^{P} \left[(\mathbf{x}_{i+1} - \mathbf{x}_i)^T \mathbf{M} (\mathbf{x}_{i+1} - \mathbf{x}_i)\right] - \frac{\beta}{P} \sum_{i=1}^{P} V(\mathbf{x}_i)\right\} \tilde{B}(\mathbf{x}_1, \ldots, \mathbf{x}_P). \tag{5}$$

The denominator of Eq. (3) takes the same form as Eq. (5) for $\hat{B} = 1$. It is straightforward to show that the estimator $\tilde{B}(\mathbf{x}_1, \ldots, \mathbf{x}_P)$ for any coordinate dependent operator $\hat{B}(\hat{\mathbf{x}})$ is

$$\tilde{B}(\mathbf{x}_1, \ldots, \mathbf{x}_P) = \frac{1}{P} \sum_{j=1}^{P} B(\mathbf{x}_j). \tag{6}$$

When $\hat{B} = \frac{1}{2} \hat{\mathbf{p}}^T \mathbf{M}^{-1} \hat{\mathbf{p}}$ is the kinetic energy operator, the primitive estimator is

$$\tilde{B}(\mathbf{x}_1, \ldots, \mathbf{x}_P) = \frac{NP}{2\beta} - \sum_{j=1}^{P} \frac{P}{2\beta^2\hbar^2} \left[(\mathbf{x}_{j+1} - \mathbf{x}_j)^T \mathbf{M} (\mathbf{x}_{j+1} - \mathbf{x}_j)\right], \tag{7}$$

and the virial version is

$$\tilde{B}(\mathbf{x}_1, \ldots, \mathbf{x}_P) = \frac{N}{2\beta} + \frac{1}{2P} \sum_{j=1}^{P} \left[(\mathbf{x}_j - \mathbf{x}^*)^T \frac{\partial V(\mathbf{x}_j)}{\partial \mathbf{x}_j}\right], \tag{8}$$

where

$$\mathbf{x}^* = \mathbf{x}_c \equiv \frac{1}{P} \sum_{j=1}^{P} \mathbf{x}_j, \tag{9}$$

or $\mathbf{x}^*$ can be any one of the P beads

$$\mathbf{x}^* = \mathbf{x}_i, \tag{10}$$

with i fixed in Eq. (8). It was suggested that the virial estimator is numerically more favorable than the primitive one as the number of beads P increases.[8]

B. Path integral molecular dynamics

Consider the staging transformation of Tuckerman *et al.*,[10,11,19]

$$\begin{aligned} \boldsymbol{\xi}_1 &= \mathbf{x}_1, \\ \boldsymbol{\xi}_j &= \mathbf{x}_j - \frac{(j-1)\mathbf{x}_{j+1} + \mathbf{x}_1}{j} \qquad \left(j = \overline{2, P}\right). \end{aligned} \tag{11}$$

Its inverse transformation takes the following convenient recursive form:

$$\begin{aligned} \mathbf{x}_1 &= \boldsymbol{\xi}_1, \\ \mathbf{x}_j &= \boldsymbol{\xi}_j + \frac{j-1}{j} \mathbf{x}_{j+1} + \frac{1}{j} \boldsymbol{\xi}_1 \qquad \left(j = \overline{2, P}\right). \end{aligned} \tag{12}$$

Its close form can be expressed as

$$\begin{aligned} \mathbf{x}_1 &= \boldsymbol{\xi}_1, \\ \mathbf{x}_j &= \boldsymbol{\xi}_1 + \sum_{k=j}^{P} \frac{j-1}{k-1} \boldsymbol{\xi}_k \qquad \left(j = \overline{2, P}\right). \end{aligned} \tag{13}$$

If one defines

$$\omega_P = \frac{\sqrt{P}}{\beta\hbar}, \tag{14}$$

Eq. (4) becomes

$$Z \overset{\xi_1 \equiv \mathbf{x}_1}{=} \lim_{\mathrm{P}\to\infty} \left(\frac{P}{2\pi\beta\hbar^2}\right)^{N\mathrm{P}/2} |\mathbf{M}|^{P/2} \int d\xi_1 \int d\xi_2 \cdots \int d\xi_P \times \exp\left\{-\beta \sum_{j=1}^{P} \left[\frac{1}{2}\omega_{\mathrm{P}}^2 \xi_j^T \bar{\mathbf{M}}_{\mathrm{j}} \xi_j + \frac{1}{P} V\left(\mathbf{x}_j\left(\xi_1,\ldots,\xi_P\right)\right)\right]\right\}, \tag{15}$$

with the (diagonal) mass matrices given by

$$\begin{aligned} \bar{\mathbf{M}}_1 &= 0, \\ \bar{\mathbf{M}}_j &= \frac{j}{j-1}\mathbf{M} \qquad \left(j = \overline{2,P}\right). \end{aligned} \tag{16}$$

If one defines

$$\phi\left(\xi_1,\ldots,\xi_P\right) = \frac{1}{P}\sum_{j=1}^{P} V\left(\mathbf{x}_j\left(\xi_1,\ldots,\xi_P\right)\right), \tag{17}$$

one then obtains the chain rule

$$\begin{aligned} \frac{\partial\phi}{\partial\xi_1} &= \sum_{i=1}^{P}\frac{\partial\phi}{\partial\mathbf{x}_i} = \frac{1}{P}\sum_{i=1}^{P} V'\left(\mathbf{x}_i\right), \\ \frac{\partial\phi}{\partial\xi_j} &= \frac{\partial\phi}{\partial\mathbf{x}_j} + \frac{j-2}{j-1}\frac{\partial\phi}{\partial\xi_{j-1}} \qquad \left(j = \overline{2,P}\right) \end{aligned} \tag{18}$$

from Eqs. (11) and (12). Employing the isomorphism strategy proposed by Chandler and Wolynes,[2] one can insert fictitious momenta $(\mathbf{p}_1,\ldots,\mathbf{p}_P)$ into Eq. (15), which leads to

$$Z \overset{\xi_1 \equiv \mathbf{x}_1}{=} \lim_{P\to\infty} \left(\frac{P}{4\pi^2\hbar^2}\right)^{N\mathrm{P}/2} |\mathbf{M}|^{P/2} \left(\prod_{j=1}^{P} |\tilde{\mathbf{M}}_j|\right)^{-1/2} \times \int \left(\prod_{j=1}^{P} d\xi_j d\mathbf{p}_j\right) \times \exp\left[-\beta H_{eff}\left(\xi_1,\ldots,\xi_P;\mathbf{p}_1,\ldots,\mathbf{p}_P\right)\right], \tag{19}$$

with the effective Hamiltonian given by

$$H_{eff}\left(\xi_1,\ldots,\xi_P;\mathbf{p}_1,\ldots,\mathbf{p}_P\right) = \sum_{j=1}^{P}\frac{1}{2}\mathbf{p}_j^T\tilde{\mathbf{M}}_j^{-1}\mathbf{p}_j + U_{eff}\left(\xi_1,\ldots,\xi_P\right), \tag{20}$$

where

$$U_{eff}\left(\xi_1,\ldots,\xi_P\right) = \sum_{j=1}^{P}\frac{1}{2}\omega_{\mathrm{P}}^2\xi_j^T\bar{\mathbf{M}}_{\mathrm{j}}\xi_j + \phi\left(\xi_1,\ldots,\xi_P\right). \tag{21}$$

The fictitious masses are chosen as

$$\begin{aligned} \tilde{\mathbf{M}}_1 &= \mathbf{M}, \\ \tilde{\mathbf{M}}_j &= \bar{\mathbf{M}}_j \qquad \left(j = \overline{2,P}\right), \end{aligned} \tag{22}$$

such that all staging modes $(\xi_2,\ldots,\xi_P)$ will move on the same time scale. The thermodynamic property Eq. (3) is then expressed as

$$\left\langle \hat{B}\right\rangle = \lim_{P\to\infty} \frac{\int\left(\prod_{j=1}^{P} d\xi_j d\mathbf{p}_j\right)\exp\left\{-\beta H_{eff}\left(\xi_1,\ldots,\xi_P;\mathbf{p}_1,\ldots,\mathbf{p}_P\right)\right\}\tilde{B}\left(\mathbf{x}_1,\ldots,\mathbf{x}_P\right)}{\int\left(\prod_{j=1}^{P} d\xi_j d\mathbf{p}_j\right)\exp\left\{-\beta H_{eff}\left(\xi_1,\ldots,\xi_P;\mathbf{p}_1,\ldots,\mathbf{p}_P\right)\right\}}. \tag{23}$$

One can sample $(\xi_1,\ldots,\xi_P,\mathbf{p}_1,\ldots,\mathbf{p}_P)$ in a molecular dynamics (MD) scheme for evaluating the thermodynamic property. That is, Eq. (23) leads to

$$\begin{aligned} \dot{\xi}_j &= \tilde{\mathbf{M}}_j^{-1}\,\mathbf{p}_j, \\ \dot{\mathbf{p}}_j &= -\omega_P^2\bar{\mathbf{M}}_j\xi_j - \frac{\partial\phi}{\partial\xi_j} \qquad \left(j = \overline{1,P}\right). \end{aligned} \tag{24}$$

The equations of motion for $(\xi_1,\ldots,\xi_P,\mathbf{p}_1,\ldots,\mathbf{p}_P)$ in Eq. (24) must be coupled to a thermostatting method to ensure a proper canonical distribution for $(\xi_1,\ldots,\xi_P,\mathbf{p}_1,\ldots,\mathbf{p}_P)$. Note that only the configurational distribution of PIMD is important in Eq. (23).

C. Algorithms for PIMD with Langevin thermostats

When a simple (white noise) Langevin dynamics is employed to the thermostat of the staging path integral variables $(\xi_1,\ldots,\xi_P,\mathbf{p}_1,\ldots,\mathbf{p}_P)$ in PIMD, Eq. (24) becomes

$$\begin{pmatrix}\dot{\xi}_j \\ \dot{\mathbf{p}}_j\end{pmatrix} = \begin{pmatrix} \tilde{\mathbf{M}}_j^{-1}\,\mathbf{p}_j \\ -\omega_P^2\bar{\mathbf{M}}_j\xi_j - \dfrac{\partial\phi}{\partial\xi_j} - \gamma_{Lang}^{(j)}\mathbf{p}_j + \sqrt{\dfrac{2\gamma_{Lang}^{(j)}}{\beta}}\left(\tilde{\mathbf{M}}_j\right)^{1/2}\boldsymbol{\eta}_j\left(t\right) \end{pmatrix} \qquad \left(j = \overline{1,P}\right). \tag{25}$$

Here $\boldsymbol{\eta}_j(t)$ is a vector. Its (white-noise) element $\eta_j^i(t)$ is an independent Gaussian-distributed random number with zero mean and unit variance $[\left\langle\eta_j^i\left(t\right)\right\rangle = 0$ and $\left\langle\eta_j^i\left(t\right)\eta_j^i\left(t'\right)\right\rangle = \delta\left(t-t'\right)]$, which is different for each physical degree of freedom $\left(i = \overline{1,N}\right)$, each staging mode $\left(j = \overline{1,P}\right)$, and each time step. The Langevin friction coefficient $\gamma_{Lang}^{(j)}$ is the same

for the staging modes $\left(j=\overline{2,P}\right)$ and all degrees of freedom $\left(i=\overline{1,N}\right)$ because they share the same frequency ω_P. The optimum value for the friction coefficient $\gamma_{Lang}^{(j)}$ is

$$\gamma_{Lang}^{opt}=\omega_P, \tag{26}$$

which offers the most efficient configurational sampling in the free particle limit for the staging variables $(\boldsymbol{\xi}_2,\ldots,\boldsymbol{\xi}_P)$[20,21] (see the Appendix A). Because the number of path integral beads P in principle approaches infinity in PIMD for obtaining exact quantum thermodynamic properties [Eq. (23)], the optimum friction coefficient γ_{Lang}^{opt} for overall sampling of the configurational distribution is then often considerably large for converged results according to Eqs. (14) and (26).

Because the harmonic force term $-\omega_P^2\bar{\mathbf{M}}_j\boldsymbol{\xi}_j$ often varies much more frequently than the force term $-\frac{\partial\phi}{\partial\boldsymbol{\xi}_j}$, Eq. (25) can be divided into three parts,

$$\begin{pmatrix}\dot{\boldsymbol{\xi}}_j\\ \dot{\mathbf{p}}_j\end{pmatrix}=\underbrace{\begin{pmatrix}\tilde{\mathbf{M}}_j^{-1}\mathbf{p}_j\\ -\omega_P^2\bar{\mathbf{M}}_j\boldsymbol{\xi}_j\end{pmatrix}}_{A}+\underbrace{\begin{pmatrix}0\\ -\dfrac{\partial\phi}{\partial\boldsymbol{\xi}_j}\end{pmatrix}}_{B}+\underbrace{\begin{pmatrix}0\\ -\gamma_{Lang}^{(j)}\mathbf{p}_j+\sigma_j(\tilde{\mathbf{M}}_j)^{1/2}\boldsymbol{\eta}_j(t)\end{pmatrix}}_{O}\quad\left(j=\overline{1,P}\right), \tag{27}$$

with $\sigma_j=\sqrt{\frac{2\gamma_{Lang}^{(j)}}{\beta}}$ and each of the three parts may be solved "exactly." In case of the harmonic part (i.e., part A), the analytical solution for a time interval Δt is

$$\begin{aligned}\boldsymbol{\xi}_1&\leftarrow\boldsymbol{\xi}_1+\tilde{\mathbf{M}}_1^{-1}\mathbf{p}_1\Delta t,\\ \begin{pmatrix}\boldsymbol{\xi}_j\\ \mathbf{p}_j\end{pmatrix}&\leftarrow\begin{pmatrix}\cos(\omega_P\Delta t)\ \mathbf{1} & \sin(\omega_P\Delta t)/\omega_P\ \tilde{\mathbf{M}}_j^{-1}\\ -\omega_P\sin(\omega_P\Delta t)\ \tilde{\mathbf{M}}_j & \cos(\omega_P\Delta t)\ \mathbf{1}\end{pmatrix}\begin{pmatrix}\boldsymbol{\xi}_j\\ \mathbf{p}_j\end{pmatrix}\quad\left(j=\overline{2,P}\right).\end{aligned} \tag{28}$$

The similar technique is often employed in MD when the harmonic system is used as the reference.[22,23] While part B leads to

$$\mathbf{p}_j\leftarrow\mathbf{p}_j-\frac{\partial\phi}{\partial\boldsymbol{\xi}_j}\Delta t, \tag{29}$$

the solution to the Ornstein-Uhlenbeck (OU) part (i.e., part O) is

$$\mathbf{p}_j\leftarrow e^{-\gamma_{Lang}^{(j)}\Delta t}\mathbf{p}_j+\sqrt{\frac{1-e^{-2\gamma_{Lang}^{(j)}\Delta t}}{\beta}}(\tilde{\mathbf{M}}_j)^{1/2}\boldsymbol{\eta}_j. \tag{30}$$

Here $\boldsymbol{\eta}_j$ is the independent Gaussian-distributed random number vector as discussed for Eq. (25).

By employing the velocity Verlet algorithm with a (white noise) Langevin thermostat for MD,[24,25] Ceriotti *et al.* constructed the PILE algorithm[17] for PIMD, which used the splitting in Eq. (27) for a time interval Δt by the composition

$$e^{\mathcal{L}\Delta t}\approx e^{\mathcal{L}_O\Delta t/2}e^{\mathcal{L}_B\Delta t/2}e^{\mathcal{L}_A\Delta t}e^{\mathcal{L}_B\Delta t/2}e^{\mathcal{L}_O\Delta t/2}, \tag{31}$$

for the phase space propagator $e^{\mathcal{L}\Delta t}$ associated to the Langevin equation. For comparing with the new integrator that will be shortly introduced, we note it OBABO according to the order of splitting. The OBABO algorithm (or equivalently PILE) for propagating the PIMD trajectory through a time interval Δt for Eq. (25) is

$$\mathbf{p}_j\leftarrow c_1^{(j)}\mathbf{p}_j+c_2^{(j)}\sqrt{\frac{1}{\beta}}(\tilde{\mathbf{M}}_j)^{1/2}\boldsymbol{\eta}_j\qquad\left(j=\overline{1,P}\right), \tag{32}$$

$$\mathbf{p}_j\leftarrow\mathbf{p}_j-\frac{\partial\phi}{\partial\boldsymbol{\xi}_j}\frac{\Delta t}{2}\qquad\left(j=\overline{1,P}\right), \tag{33}$$

$$\begin{aligned}\boldsymbol{\xi}_1&\leftarrow\boldsymbol{\xi}_1+\tilde{\mathbf{M}}_1^{-1}\mathbf{p}_1\Delta t,\\ \begin{pmatrix}\boldsymbol{\xi}_j\\ \mathbf{p}_j\end{pmatrix}&\leftarrow\begin{pmatrix}\cos(\omega_P\Delta t)\ \mathbf{1} & \sin(\omega_P\Delta t)/\omega_P\ \tilde{\mathbf{M}}_j^{-1}\\ -\omega_P\sin(\omega_P\Delta t)\ \tilde{\mathbf{M}}_j & \cos(\omega_P\Delta t)\ \mathbf{1}\end{pmatrix}\begin{pmatrix}\boldsymbol{\xi}_j\\ \mathbf{p}_j\end{pmatrix}\quad\left(j=\overline{2,P}\right),\end{aligned} \tag{34}$$

$$\mathbf{p}_j\leftarrow\mathbf{p}_j-\frac{\partial\phi}{\partial\boldsymbol{\xi}_j}\frac{\Delta t}{2}\qquad\left(j=\overline{1,P}\right), \tag{35}$$

$$\mathbf{p}_j\leftarrow c_1^{(j)}\mathbf{p}_j+c_2^{(j)}\sqrt{\frac{1}{\beta}}(\tilde{\mathbf{M}}_j)^{1/2}\boldsymbol{\eta}_j\qquad\left(j=\overline{1,P}\right). \tag{36}$$

Here the independent Gaussian-distributed random number vector $\boldsymbol{\eta}_j$ is different for each invocation of Eq. (32) or Eq. (36). The coefficients $c_1^{(j)}$ and $c_2^{(j)}$ are

$$\begin{aligned} c_1^{(j)} &= \exp\left[-\gamma_{Lang}^{(j)}\Delta t/2\right] \\ c_2^{(j)} &= \sqrt{1-\left(c_1^{(j)}\right)^2} \end{aligned} \qquad \left(j=\overline{1,P}\right), \tag{37}$$

respectively. While the forces in Eq. (33) are obtained from the previous time step, those in Eq. (35) at the current time step can be efficiently evaluated by the chain rule Eq. (18). The OBABO (or PILE) algorithm [Eqs. (32)–(36)] for staging PIMD has already been employed in Ref. 20.

Leimkuhler and Matthews have recently tested various algorithms for thermostatting MD with Langevin dynamics.[26–28] It is suggested that the splitting

$$e^{\mathcal{L}\Delta t} \approx e^{\mathcal{L}_B\Delta t/2}e^{\mathcal{L}_A\Delta t/2}e^{\mathcal{L}_O\Delta t}e^{\mathcal{L}_A\Delta t/2}e^{\mathcal{L}_B\Delta t/2} \tag{38}$$

leads to the most efficient MD algorithm for sampling the configurational space in the high friction limit.[26,27] When the order of splitting Eq. (38) is implemented to construct a PIMD algorithm for Eq. (27), we note it BAOAB. Such a BAOAB integrator for propagating the PIMD trajectory through a time interval Δt for Eq. (25) is

$$\mathbf{p}_j \leftarrow \mathbf{p}_j - \frac{\partial\phi}{\partial\boldsymbol{\xi}_j}\frac{\Delta t}{2} \qquad \left(j=\overline{1,P}\right), \tag{39}$$

$$\begin{aligned} \boldsymbol{\xi}_1 &\leftarrow \boldsymbol{\xi}_1 + \tilde{\mathbf{M}}_1^{-1}\mathbf{p}_1\frac{\Delta t}{2}, \\ \begin{pmatrix}\boldsymbol{\xi}_j\\ \mathbf{p}_j\end{pmatrix} &\leftarrow \begin{pmatrix}\cos\left(\omega_P\Delta t/2\right)\ \mathbf{1} & \sin\left(\omega_P\Delta t/2\right)/\omega_P\ \tilde{\mathbf{M}}_j^{-1}\\ -\omega_P\sin\left(\omega_P\Delta t/2\right)\ \tilde{\mathbf{M}}_j & \cos\left(\omega_P\Delta t/2\right)\ \mathbf{1}\end{pmatrix}\begin{pmatrix}\boldsymbol{\xi}_j\\ \mathbf{p}_j\end{pmatrix} \quad \left(j=\overline{2,P}\right), \end{aligned} \tag{40}$$

$$\mathbf{p}_j \leftarrow \tilde{c}_1^{(j)}\mathbf{p}_j + \tilde{c}_2^{(j)}\sqrt{\frac{1}{\beta}}\left(\tilde{\mathbf{M}}_j\right)^{1/2}\boldsymbol{\eta}_j \qquad \left(j=\overline{1,P}\right), \tag{41}$$

$$\begin{aligned} \boldsymbol{\xi}_1 &\leftarrow \boldsymbol{\xi}_1 + \tilde{\mathbf{M}}_1^{-1}\mathbf{p}_1\frac{\Delta t}{2}, \\ \begin{pmatrix}\boldsymbol{\xi}_j\\ \mathbf{p}_j\end{pmatrix} &\leftarrow \begin{pmatrix}\cos\left(\omega_P\Delta t/2\right)\ \mathbf{1} & \sin\left(\omega_P\Delta t/2\right)/\omega_P\ \tilde{\mathbf{M}}_j^{-1}\\ -\omega_P\sin\left(\omega_P\Delta t/2\right)\ \tilde{\mathbf{M}}_j & \cos\left(\omega_P\Delta t/2\right)\ \mathbf{1}\end{pmatrix}\begin{pmatrix}\boldsymbol{\xi}_j\\ \mathbf{p}_j\end{pmatrix} \quad \left(j=\overline{2,P}\right), \end{aligned} \tag{42}$$

$$\mathbf{p}_j \leftarrow \mathbf{p}_j - \frac{\partial\phi}{\partial\boldsymbol{\xi}_j}\frac{\Delta t}{2} \qquad \left(j=\overline{1,P}\right), \tag{43}$$

where the independent Gaussian-distributed random number vector $\boldsymbol{\eta}_j$ is different for each invocation of Eq. (41), and the coefficients are

$$\begin{aligned} \tilde{c}_1^{(j)} &= \exp\left[-\gamma_{Lang}^{(j)}\Delta t\right], \\ \tilde{c}_2^{(j)} &= \sqrt{1-\left(\tilde{c}_1^{(j)}\right)^2} \end{aligned} \qquad \left(j=\overline{1,P}\right). \tag{44}$$

The implementation of the BAOAB algorithm [Eqs. (39)–(43)] is very simple, which has already been done in our earlier work.[21,29]

D. Accuracy of the PIMD integrators

BAOAB and OBABO approach each other in the limit $\Delta t \to 0$. Both BAOAB and OBABO exploit an analytic knowledge of path integral staging mode frequencies in the free particle limit [Eq. (26)]. It is trivial to verify that either of BAOAB and OBABO is exact in the free particle limit.

Eq. (27) can be expressed in a more compact form as

$$\begin{pmatrix}\dot{\boldsymbol{\xi}}\\ \dot{\mathbf{p}}\end{pmatrix} = \underbrace{\begin{pmatrix}\tilde{\mathbf{M}}^{-1}\,\mathbf{p}\\ -\omega_P^2\tilde{\mathbf{M}}\boldsymbol{\xi}\end{pmatrix}}_{A} + \underbrace{\begin{pmatrix}0\\ -\dfrac{\partial\phi}{\partial\boldsymbol{\xi}}\end{pmatrix}}_{B} + \underbrace{\begin{pmatrix}0\\ -\boldsymbol{\gamma}_{Lang}\mathbf{p}+\boldsymbol{\sigma}\,\tilde{\mathbf{M}}^{1/2}\boldsymbol{\eta}\,(t)\end{pmatrix}}_{O}. \tag{45}$$

Here,

$$\boldsymbol{\xi} = \begin{pmatrix}\boldsymbol{\xi}_1\\ \vdots\\ \boldsymbol{\xi}_P\end{pmatrix},\ \mathbf{p} = \begin{pmatrix}\mathbf{p}_1\\ \vdots\\ \mathbf{p}_P\end{pmatrix},$$

$$\bar{\mathbf{M}} = \begin{pmatrix}\bar{\mathbf{M}}_1 & & \\ & \ddots & \\ & & \bar{\mathbf{M}}_P\end{pmatrix},\ \tilde{\mathbf{M}} = \begin{pmatrix}\tilde{\mathbf{M}}_1 & & \\ & \ddots & \\ & & \tilde{\mathbf{M}}_P\end{pmatrix},$$

$$\boldsymbol{\eta}(t) = \begin{pmatrix}\boldsymbol{\eta}_1(t)\\ \vdots\\ \boldsymbol{\eta}_P(t)\end{pmatrix},$$

$$\boldsymbol{\gamma}_{Lang} = \begin{pmatrix}\gamma_{Lang}^{(1)}\cdot\mathbf{1}_{N\times N} & & \\ & \ddots & \\ & & \gamma_{Lang}^{(P)}\cdot\mathbf{1}_{N\times N}\end{pmatrix}$$

and

$$\boldsymbol{\sigma} = \begin{pmatrix}\sigma_1\cdot\mathbf{1}_{N\times N} & & \\ & \ddots & \\ & & \sigma_P\cdot\mathbf{1}_{N\times N}\end{pmatrix}.$$

Eq. (20) then becomes

$$H_{eff}(\boldsymbol{\xi};\ \mathbf{p}) = \frac{1}{2}\mathbf{p}^T\tilde{\mathbf{M}}^{-1}\mathbf{p} + \frac{1}{2}\omega_P^2\boldsymbol{\xi}^T\bar{\mathbf{M}}\boldsymbol{\xi} + \phi(\boldsymbol{\xi}) = \frac{1}{2}\mathbf{p}^T\tilde{\mathbf{M}}^{-1}\mathbf{p} + U_{eff}(\boldsymbol{\xi}). \quad (46)$$

The density evolves according to the Fokker-Planck or forward Kolmogorov equation,

$$\frac{\partial\rho}{\partial t} = \mathcal{L}\rho, \quad (47)$$

where the relevant Kolmogorov operator $\mathcal{L}$ is defined by

$$\mathcal{L} = \mathcal{L}_{LD} = \mathcal{L}_A + \mathcal{L}_B + \mathcal{L}_O, \quad (48)$$

with

$$\mathcal{L}_A\rho = -\mathbf{p}^T\tilde{\mathbf{M}}^{-1}\frac{\partial}{\partial\boldsymbol{\xi}}\rho + \omega_P^2\boldsymbol{\xi}^T\bar{\mathbf{M}}\frac{\partial}{\partial\mathbf{p}}\rho, \quad (49)$$

$$\mathcal{L}_B\rho = \left(\frac{\partial\phi}{\partial\boldsymbol{\xi}}\right)^T\frac{\partial}{\partial\mathbf{p}}\rho, \quad (50)$$

$$\mathcal{L}_O\rho = \frac{\partial}{\partial\mathbf{p}}\cdot\left(\boldsymbol{\gamma}_{Lang}\mathbf{p}\rho\right) + \frac{1}{2}\frac{\partial}{\partial\mathbf{p}}\cdot\left(\boldsymbol{\sigma}^2\tilde{\mathbf{M}}\frac{\partial\rho}{\partial\mathbf{p}}\right). \quad (51)$$

It is straightforward to verify that

$$\rho_{eq}(\boldsymbol{\xi};\ \mathbf{p}) = Z_{eff}^{-1}\exp\left[-\beta H_{eff}(\boldsymbol{\xi};\ \mathbf{p})\right] \quad (52)$$

is a steady state of Eq. (47). Here Z_{eff} is the normalization constant of the density distribution, $Z_{eff} = \int d\boldsymbol{\xi}d\mathbf{p}\exp\{-\beta H_{eff}(\boldsymbol{\xi};\ \mathbf{p})\} = \int\left(\prod_{j=1}^{P}d\boldsymbol{\xi}_j d\mathbf{p}_j\right)\exp\{-\beta H_{eff}(\boldsymbol{\xi}_1,\ldots,\boldsymbol{\xi}_P;\mathbf{p}_1,\ldots,\mathbf{p}_P)\}$.

The exact phase space propagator for a time interval Δt for Eq. (47) is $e^{\mathcal{L}_{LD}\Delta t}$. When the BAOAB integrator [Eq. (38)] is employed, the "approximate" phase space propagator is

$$e^{\mathcal{L}_B\Delta t/2}e^{\mathcal{L}_A\Delta t/2}e^{\mathcal{L}_O\Delta t}e^{\mathcal{L}_A\Delta t/2}e^{\mathcal{L}_B\Delta t/2} = e^{\mathcal{L}_{BAOAB}\Delta t}. \quad (53)$$

Using the Baker–Campbell–Hausdorff formula to expand the left-hand side of Eq. (53), one then obtains

$$\begin{aligned}\mathcal{L}_{BAOAB} &= \mathcal{L}_A + \mathcal{L}_B + \mathcal{L}_O + \frac{1}{24}\{2[\mathcal{L}_O,[\mathcal{L}_O,\mathcal{L}_A+\mathcal{L}_B]] \\ &\quad + 2[\mathcal{L}_A,[\mathcal{L}_A,\mathcal{L}_B]] + 2[\mathcal{L}_O,[\mathcal{L}_A,\mathcal{L}_B]] \\ &\quad + 2[\mathcal{L}_A,[\mathcal{L}_O,\mathcal{L}_B]] - [\mathcal{L}_A,[\mathcal{L}_A,\mathcal{L}_O]] \\ &\quad - [\mathcal{L}_B,[\mathcal{L}_B,\mathcal{L}_O]] - [\mathcal{L}_B,[\mathcal{L}_B,\mathcal{L}_A]]\}\Delta t^2 + O(\Delta t^4) \\ &= \mathcal{L}_{LD} + \mathcal{L}_2^{BAOAB}\Delta t^2 + O(\Delta t^4). \end{aligned} \quad (54)$$

It is straightforward to show that

$$\begin{aligned}\mathcal{L}_2^{BAOAB}\rho_{eq} = \rho_{eq}\Bigg[&\frac{1}{4}\left(\frac{\partial}{\partial\boldsymbol{\xi}}\cdot\left(\boldsymbol{\gamma}_{Lang}\tilde{\mathbf{M}}^{-1}\frac{\partial\phi}{\partial\boldsymbol{\xi}}\right) - \beta\mathbf{p}^T\boldsymbol{\gamma}_{Lang}\tilde{\mathbf{M}}^{-1}\phi''\tilde{\mathbf{M}}^{-1}\mathbf{p}\right) \\ &+ \frac{\beta}{4}\mathbf{p}^T\tilde{\mathbf{M}}^{-1}\phi''\tilde{\mathbf{M}}^{-1}\frac{\partial\phi}{\partial\boldsymbol{\xi}} - \frac{\beta}{12}\mathbf{p}^T\tilde{\mathbf{M}}^{-1}\frac{\partial}{\partial\boldsymbol{\xi}}\left(\mathbf{p}^T\tilde{\mathbf{M}}^{-1}\phi''\tilde{\mathbf{M}}^{-1}\mathbf{p}\right) \\ &+ \frac{\beta}{12}\omega_P^2\left(\mathbf{p}^T\tilde{\mathbf{M}}^{-1}\bar{\mathbf{M}}\tilde{\mathbf{M}}^{-1}\frac{\partial\phi}{\partial\boldsymbol{\xi}} + 3\mathbf{p}^T\tilde{\mathbf{M}}^{-1}\phi''\bar{\mathbf{M}}\tilde{\mathbf{M}}^{-1}\boldsymbol{\xi}\right)\Bigg], \end{aligned} \quad (55)$$

where $\phi'' = \frac{\partial^2\phi}{\partial\boldsymbol{\xi}^2}$ is a Hessian matrix.

Consider the steady state ρ^{BAOAB} for the relevant Kolmogorov operator $\mathcal{L}_{BAOAB}$, which satisfies

$$\frac{\partial\rho^{BAOAB}}{\partial t} = \mathcal{L}_{BAOAB}\rho^{BAOAB} = 0. \quad (56)$$

Assume that ρ^{BAOAB} takes the form

$$\rho^{BAOAB} = \rho_{eq}\left[1 - \beta\omega_P^2\Delta t^2 f_2^{BAOAB} + O(\omega_P^4\Delta t^4)\right]. \quad (57)$$

Substituting Eqs. (54) and (57) into Eq. (56) leads to

$$\mathcal{L}_{LD}(\rho_{eq}f_2^{BAOAB}) = \frac{1}{\beta\omega_P^2}\mathcal{L}_2^{BAOAB}\rho_{eq}. \quad (58)$$

When Eq. (26) is used as the optimum friction coefficients, $\boldsymbol{\gamma}_{Lang}$ is then expressed as $\boldsymbol{\gamma}_{Lang} = \omega_P\boldsymbol{\gamma}_1$. Since the number of beads P is often large, $\varepsilon = 1/\omega_P$ is small. f_2^{BAOAB} can be expressed as

$$f_2^{BAOAB} = f_{2,0}^{BAOAB} + f_{2,1}^{BAOAB}\varepsilon + f_{2,2}^{BAOAB}\varepsilon^2 + O(\varepsilon^3). \quad (59)$$

Substituting Eq. (59) into Eq. (58) and then dividing both sides by ω_P^2, one finds

$$\begin{aligned}&(\mathcal{L}_0 + \varepsilon\mathcal{L}_1 + \varepsilon^2\mathcal{L}_2)\left[f_{2,0}^{BAOAB} + f_{2,1}^{BAOAB}\varepsilon + f_{2,2}^{BAOAB}\varepsilon^2 + O(\varepsilon^3)\right] \\ &\quad = g_2^{BAOAB}\varepsilon^2 + g_3^{BAOAB}\varepsilon^3 + g_4^{BAOAB}\varepsilon^4, \end{aligned} \quad (60)$$

where

$$\mathcal{L}_0\rho = \boldsymbol{\xi}^T\bar{\mathbf{M}}\frac{\partial}{\partial\mathbf{p}}\rho, \quad (61)$$

$$\mathcal{L}_1\rho = \frac{1}{\beta}\frac{\partial}{\partial\mathbf{p}}\cdot\left(\boldsymbol{\gamma}_1\tilde{\mathbf{M}}\frac{\partial\rho}{\partial\mathbf{p}}\right) - \mathbf{p}^T\boldsymbol{\gamma}_1\frac{\partial\rho}{\partial\mathbf{p}}, \quad (62)$$

$$\mathcal{L}_2\rho = \left(\frac{\partial\phi}{\partial\boldsymbol{\xi}}\right)^T\frac{\partial\rho}{\partial\mathbf{p}} - \mathbf{p}^T\tilde{\mathbf{M}}^{-1}\frac{\partial\rho}{\partial\boldsymbol{\xi}}, \quad (63)$$

$$g_2^{BAOAB} = \frac{1}{12}\left(\mathbf{p}^T\tilde{\mathbf{M}}^{-1}\bar{\mathbf{M}}\tilde{\mathbf{M}}^{-1}\frac{\partial\phi}{\partial\boldsymbol{\xi}} + 3\mathbf{p}^T\tilde{\mathbf{M}}^{-1}\phi''\bar{\mathbf{M}}\tilde{\mathbf{M}}^{-1}\boldsymbol{\xi}\right), \quad (64)$$

$$g_3^{BAOAB} = \frac{1}{4}\left(\frac{1}{\beta}\frac{\partial}{\partial\boldsymbol{\xi}}\cdot\left(\boldsymbol{\gamma}_1\tilde{\mathbf{M}}^{-1}\frac{\partial\phi}{\partial\boldsymbol{\xi}}\right) - \mathbf{p}^T\boldsymbol{\gamma}_1\tilde{\mathbf{M}}^{-1}\phi''\tilde{\mathbf{M}}^{-1}\mathbf{p}\right), \quad (65)$$

$$\begin{aligned}g_4^{BAOAB} = &\frac{1}{4}\mathbf{p}^T\tilde{\mathbf{M}}^{-1}\phi''\tilde{\mathbf{M}}^{-1}\frac{\partial\phi}{\partial\boldsymbol{\xi}} \\ &- \frac{1}{12}\mathbf{p}^T\tilde{\mathbf{M}}^{-1}\frac{\partial}{\partial\boldsymbol{\xi}}\left(\mathbf{p}^T\tilde{\mathbf{M}}^{-1}\phi''\tilde{\mathbf{M}}^{-1}\mathbf{p}\right). \end{aligned} \quad (66)$$

Equating powers of ε in Eq. (60), one obtains

$$\begin{aligned}
&\mathcal{L}_0 f_{2,0}^{BAOAB} = 0,\\
&\mathcal{L}_1 f_{2,0}^{BAOAB} + \mathcal{L}_0 f_{2,1}^{BAOAB} = 0,\\
&\mathcal{L}_0 f_{2,2}^{BAOAB} + \mathcal{L}_1 f_{2,1}^{BAOAB} + \mathcal{L}_2 f_{2,0}^{BAOAB} = g_2^{BAOAB},\\
&\cdots
\end{aligned} \tag{67}$$

Truncating at the 2nd order of ε, one finds a solution of Eq. (67)

$$\begin{aligned}
f_{2,0}^{BAOAB} &= -\frac{1}{12}\phi + G_0,\\
f_{2,1}^{BAOAB} &= \frac{1}{12}\mathbf{p}^T\boldsymbol{\gamma}_1^{-1}\tilde{\mathbf{M}}^{-1}(\mathbf{1}-\bar{\mathbf{M}}\tilde{\mathbf{M}}^{-1})\frac{\partial\phi}{\partial\boldsymbol{\xi}} - G_1(\boldsymbol{\xi}),\\
f_{2,2}^{BAOAB} &= \frac{1}{8}\left[\mathbf{p}^T\tilde{\mathbf{M}}^{-1}\phi''\tilde{\mathbf{M}}^{-1}\mathbf{p} - \frac{1}{\beta}\frac{\partial}{\partial\boldsymbol{\xi}}\cdot\left(\tilde{\mathbf{M}}^{-1}\frac{\partial\phi}{\partial\boldsymbol{\xi}}\right)\right] - G_2(\boldsymbol{\xi}).
\end{aligned} \tag{68}$$

Here G_0 is a constant, and $G_1(\boldsymbol{\xi})$ and $G_2(\boldsymbol{\xi})$ are functions to be determined by the equations for the 3rd and higher orders of ε in Eq. (67). (In the free particle limit, G_0, $G_1(\boldsymbol{\xi})$, and $G_2(\boldsymbol{\xi})$ all approach zero.)

Note that only the configurational distribution of PIMD is useful, i.e.,

$$\rho_{eq}^{config}(\boldsymbol{\xi}) = \int d\mathbf{p}\rho_{eq}(\boldsymbol{\xi};\mathbf{p}) = \frac{1}{Z^{config}}\exp\left[-\beta U_{eff}(\boldsymbol{\xi})\right], \tag{69}$$

with a new normalization coefficient Z^{config}. Integration of ρ^{BAOAB} [Eq. (57)] over $\mathbf{p}$ produces

$$\begin{aligned}
\rho_{BAOAB}^{config}(\boldsymbol{\xi}) = \rho_{eq}^{config}(\boldsymbol{\xi})\{1 &+ \beta\omega_P^2\Delta t^2[(\phi/12 - G_0)\\
&+ \varepsilon G_1(\boldsymbol{\xi}) + \varepsilon^2 G_2(\boldsymbol{\xi}) + O(\varepsilon^3)] + O(\omega_P^4\Delta t^4)\}.
\end{aligned} \tag{70}$$

It is difficult to analyze Eq. (70) for general systems. Consider a harmonic oscillator

$$V(\mathbf{x}) = \frac{1}{2}(\mathbf{x}-\mathbf{x}_{eq})^T\mathbf{A}(\mathbf{x}-\mathbf{x}_{eq}), \tag{71}$$

where $\mathbf{A}$ is a symmetric positive-definite matrix. Eq. (17) then becomes

$$\phi = \frac{1}{2}(\boldsymbol{\xi}-\boldsymbol{\xi}_{eq})^T\mathbf{K}(\boldsymbol{\xi}-\boldsymbol{\xi}_{eq}). \tag{72}$$

Here $\boldsymbol{\xi} = \mathbf{S}\begin{pmatrix}\mathbf{x}_1\\ \vdots\\ \mathbf{x}_P\end{pmatrix}$,

$$\boldsymbol{\xi}_{eq} = \mathbf{S}\begin{pmatrix}\mathbf{x}_{eq}\\ \vdots\\ \mathbf{x}_{eq}\end{pmatrix} = \begin{pmatrix}\mathbf{x}_{eq}\\ 0\\ \vdots\\ 0\end{pmatrix}, \tag{73}$$

and the symmetric positive-definite matrix

$$\mathbf{K} = \frac{1}{P}(\mathbf{S}^{-1})^T\begin{pmatrix}\mathbf{A} & & \\ & \ddots & \\ & & \mathbf{A}\end{pmatrix}(\mathbf{S}^{-1}), \tag{74}$$

with the staging transformation matrix

$$\mathbf{S} = \begin{pmatrix}
\mathbf{1} & 0 & 0 & \cdots & 0\\
-\frac{\mathbf{1}}{\mathbf{2}} & \mathbf{1} & -\frac{\mathbf{1}}{\mathbf{2}} & \ddots & \vdots\\
\vdots & 0 & \ddots & \ddots & 0\\
-\frac{\mathbf{1}}{\mathbf{P-1}} & \vdots & 0 & \mathbf{1} & -\frac{\mathbf{P-2}}{\mathbf{P-1}}\\
\mathbf{-1} & 0 & \cdots & 0 & \mathbf{1}
\end{pmatrix} \tag{75}$$

and its inverse

$$\mathbf{S}^{-1} = \begin{pmatrix}
\mathbf{1} & 0 & 0 & 0 & \cdots & 0\\
\mathbf{1} & \mathbf{1} & \frac{\mathbf{1}}{\mathbf{2}} & \frac{\mathbf{1}}{\mathbf{3}} & \cdots & \frac{\mathbf{1}}{\mathbf{P-1}}\\
\mathbf{1} & 0 & \mathbf{1} & \frac{\mathbf{2}}{\mathbf{3}} & \cdots & \frac{\mathbf{2}}{\mathbf{P-1}}\\
\vdots & \vdots & \ddots & \ddots & & \vdots\\
\mathbf{1} & 0 & \cdots & 0 & \mathbf{1} & \frac{\mathbf{P-2}}{\mathbf{P-1}}\\
\mathbf{1} & 0 & \cdots & & 0 & \mathbf{1}
\end{pmatrix}. \tag{76}$$

Each nonzero number in Eq. (75) or (76) represents a diagonal $N\times N$ matrix. Because Eq. (16) and Eq. (73) lead to

$$\bar{\mathbf{M}}\boldsymbol{\xi}_{eq} = \begin{pmatrix}0 & & & \\ & \bar{\mathbf{M}}_2 & & \\ & & \ddots & \\ & & & \bar{\mathbf{M}}_P\end{pmatrix}\begin{pmatrix}\mathbf{x}_{eq}\\ 0\\ \vdots\\ 0\end{pmatrix} = 0, \tag{77}$$

Eq. (21) then becomes

$$U_{eff}(\boldsymbol{\xi}) = \frac{1}{2}(\boldsymbol{\xi}-\boldsymbol{\xi}_{eq})^T\boldsymbol{\Omega}(\boldsymbol{\xi}-\boldsymbol{\xi}_{eq}), \tag{78}$$

where

$$\boldsymbol{\Omega} = \omega_P^2\bar{\mathbf{M}} + \mathbf{K} \tag{79}$$

is a symmetric positive-definite matrix.

It is straightforward to verify that Eq. (70) becomes

$$\begin{aligned}
\rho_{BAOAB}^{config}(\boldsymbol{\xi}) = \rho_{eq}^{config}(\boldsymbol{\xi})\Bigg\{1 &+ \beta\omega_P^2\Delta t^2\left[\frac{1}{24}(\boldsymbol{\xi}-\boldsymbol{\xi}_{eq})^T\right.\\
&\left.\mathbf{K}(\boldsymbol{\xi}-\boldsymbol{\xi}_{eq}) - \frac{1}{24\beta}\mathrm{Tr}\left(\mathbf{K}\boldsymbol{\Omega}^{-1}\right) + O(\varepsilon)\right]\\
&+ O(\omega_P^4\Delta t^4)\Bigg\},
\end{aligned} \tag{80}$$

while truncating at the 0-th order of ε for the term associated with $\omega_P^2\Delta t^2$. Eq. (80) is a normalized density distribution.

Similarly, the normalized configurational distribution given by OBABO is

$$\rho^{config}_{OBABO}(\boldsymbol{\xi}) = \rho^{config}_{eq}(\boldsymbol{\xi})\left\{1+\beta\omega_P^2\Delta t^2\left[\left(\frac{1}{8}\boldsymbol{\xi}^T\bar{\mathbf{M}}\tilde{\mathbf{M}}^{-1}\frac{\partial\phi}{\partial\boldsymbol{\xi}}-\frac{1}{6}\phi+\tilde{G}_0\right)\right.\right.$$
$$\left.\left.+\varepsilon\tilde{G}_1(\boldsymbol{\xi})+\varepsilon^2\left(\frac{1}{8}\left(\frac{\partial\phi}{\partial\boldsymbol{\xi}}\right)^T\tilde{\mathbf{M}}^{-1}\frac{\partial\phi}{\partial\boldsymbol{\xi}}-\frac{1}{8}\frac{1}{\beta}\frac{\partial}{\partial\boldsymbol{\xi}}\cdot\left(\tilde{\mathbf{M}}^{-1}\frac{\partial\phi}{\partial\boldsymbol{\xi}}\right)+\tilde{G}_2(\boldsymbol{\xi})\right)+O\left(\varepsilon^3\right)\right]+O\left(\omega_P^4\Delta t^4\right)\right\}. \quad (81)$$

It is easy to show that Eq. (81) for the harmonic system [Eq. (71) or Eq. (72)] becomes

$$\rho^{config}_{OBABO}(\boldsymbol{\xi}) = \rho^{config}_{eq}(\boldsymbol{\xi})\left\{1+\beta\omega_P^2\Delta t^2\left[(\boldsymbol{\xi}-\boldsymbol{\xi}_{eq})^T\left(\frac{1}{4}\bar{\mathbf{M}}\tilde{\mathbf{M}}^{-1}-\frac{1}{12}\mathbf{1}\right)\mathbf{K}(\boldsymbol{\xi}-\boldsymbol{\xi}_{eq})\right.\right.$$
$$\left.\left.-\frac{1}{\beta}\mathrm{Tr}\left(\left(\frac{1}{4}\bar{\mathbf{M}}\tilde{\mathbf{M}}^{-1}-\frac{1}{12}\mathbf{1}\right)\mathbf{K}\boldsymbol{\Omega}^{-1}\right)+O(\varepsilon)\right]+O\left(\omega_P^4\Delta t^4\right)\right\}, \quad (82)$$

while truncating at the 0-th order of ε for the term associated with $\omega_P^2\Delta t^2$.

Comparing Eq. (82) to Eq. (80), the error (of the configurational distribution) produced by OBABO is increased by approximately a factor of 4 of that by BAOAB for the harmonic system. It is trivial to extend the BAOAB algorithm and the error analysis to normal mode PIMD, which leads to the similar conclusion (as shown in the supplementary material[18]).

III. RESULTS AND DISCUSSIONS

We apply the two PIMD integrators to three benchmark realistic molecular systems—the water molecule (H_2O) with an accurate PES,[30] liquid *para*-hydrogen with the Silvera-Goldman (SG) potential,[31] and liquid water with an *ab initio* based flexible, polarizable force field.[32] Both the primitive and the virial estimators [Eqs. (7) and (8)] are employed to calculate the average kinetic energy. The average potential energy is also computed. These thermodynamic properties are collected as a function of the time interval of the PIMD simulation. In practice, when the number of beads P is large enough and the time interval Δt is small enough, both BAOAB and OBABO lead to the same converged results, so does the primitive and virial estimators.

A. The H_2O molecule

We first apply the two integrators to simulate H_2O with the accurate PES developed by Partridge and Schwenke from extensive *ab initio* calculations and experimental data.[30] As the explicit form of the PES is available, that of the force can be expressed. $P = 640$ path integral beads are used in PIMD for $T = 100$ K, while $P = 256$ for $T = 300$ K. After equilibrating the molecular system, 32 PIMD trajectories with each propagated up to ~4.84 ns are used for estimating thermodynamic properties. While the time interval for PIMD for 300 K ranges from ~0.024 fs to ~0.39 fs (1–16 a.u.), that for 100 K is from ~0.012 fs to ~0.32 fs (0.5–13 a.u.).

Fig. 1 demonstrates the results for the thermodynamic properties using different time intervals of PIMD for H_2O at $T = 300$ K, while Fig. 2 does so for $T = 100$ K. The performance of BAOAB and that of OBABO are examined. Figs. 1 and 2 show that BAOAB and OBABO approach the same results as the time interval is decreased. This agrees with the fact that both integrators are in principle equivalent as the time interval approaches zero. Figs. 1(a) and 2(a) also show that the primitive estimator for the kinetic energy agrees well with the virial estimator when the time interval is small. When the number of path integral beads P is reasonably large, the primitive estimator in principle approaches the virial one as the time interval Δt of PIMD approaches zero. The difference between the results of the primitive and virial estimators ΔE_{kin} is then a reasonable quantity for measuring the behavior of the integrator for PIMD. The fully converged result for either $\left\langle\hat{\mathbf{p}}^T\mathbf{M}^{-1}\hat{\mathbf{p}}\right\rangle/(2N_{atom}k_B)$ or $\langle V(\hat{\mathbf{x}})\rangle/(N_{atom}k_B)$ is obtained at $\Delta t = 1$ a.u.

More importantly, Figs. 1 and 2 demonstrate that BAOAB is more accurate and robust than OBABO as the time interval Δt increases. While the absolute deviation of the average potential energy per atom $\langle V(\hat{\mathbf{x}})\rangle/(N_{atom}k_B)$ from the converged result for OBABO at $T = 300$ K is ~1 K for $\Delta t = 2$ a.u. and ~37 K for $\Delta t = 10$ a.u. (Fig. 1(c)), that at $T = 100$ K is ~0.8 K and ~32 K, respectively (Fig. 2(c)). For comparison, the same property for BAOAB at $T = 300$ K is only ~0.1 K for $\Delta t = 2$ a.u. and ~1 K for $\Delta t = 10$ a.u. (Fig. 1(c)), that at $T = 100$ K is only ~0.2 K and ~0.3 K, respectively (Fig. 2(c)). As the time interval increases, the error of deviation from the converged result of OBABO is about an order of magnitude (or more) larger than that of BAOAB. The trend is similar for the average kinetic energy per atom $\left\langle\hat{\mathbf{p}}^T\mathbf{M}^{-1}\hat{\mathbf{p}}\right\rangle/(2N_{atom}k_B)$ (by either the primitive or virial estimator) or for the difference between the two estimators ΔE_{kin} as suggested by Figs. 1(a) and 1(b) and 2(a) and 2(b).

B. Liquid *para*-hydrogen

Liquid *para*-hydrogen is usually described by the Silvera-Goldman (SG) model,[31] an isotropic pair potential in which the *para*-hydrogen molecule is treated as a sphere particle because the temperature of liquid *para*-hydrogen is too low for any rotational state other than J = 0 to be populated. Liquid *para*-hydrogen has served as a benchmark system to test quantum methods. We apply the two PIMD integrators to two state points $T = 25$ K, $\upsilon = 31.7$ cm^{3}mol^{-1} and $T = 14$ K, $\upsilon = 25.6$ cm^{3}mol^{-1} under nearly zero external pressure. PIMD simulations are carried out for a system of

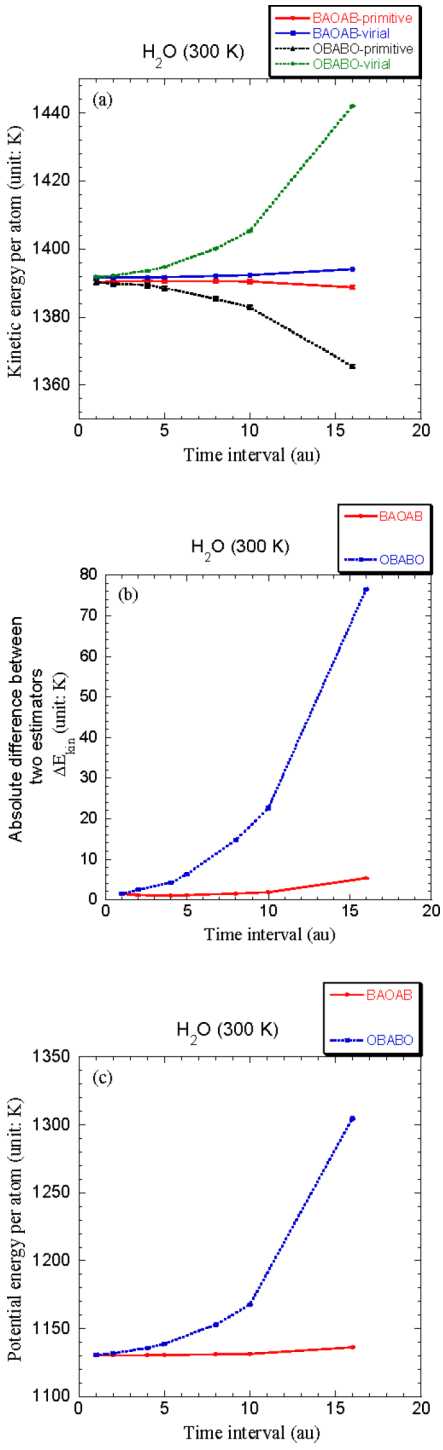

FIG. 1. PIMD results using different time intervals for H_2O at T = 300 K. (a) The average kinetic energy per atom $\langle \hat{\mathbf{p}}^T \mathbf{M}^{-1} \hat{\mathbf{p}} \rangle / (2N_{atom}k_B)$ (unit: Kelvin). Both primitive and virial estimators are used. (b) Difference between the primitive and virial estimators. (unit: Kelvin). (c) The average potential energy per atom $\langle V(\hat{\mathbf{x}}) \rangle / (N_{atom}k_B)$ (unit: Kelvin). Solid line: BAOAB results. Dotted line: OBABO results. The unit of the time interval is atomic unit (a.u.). Statistical error bars are included.

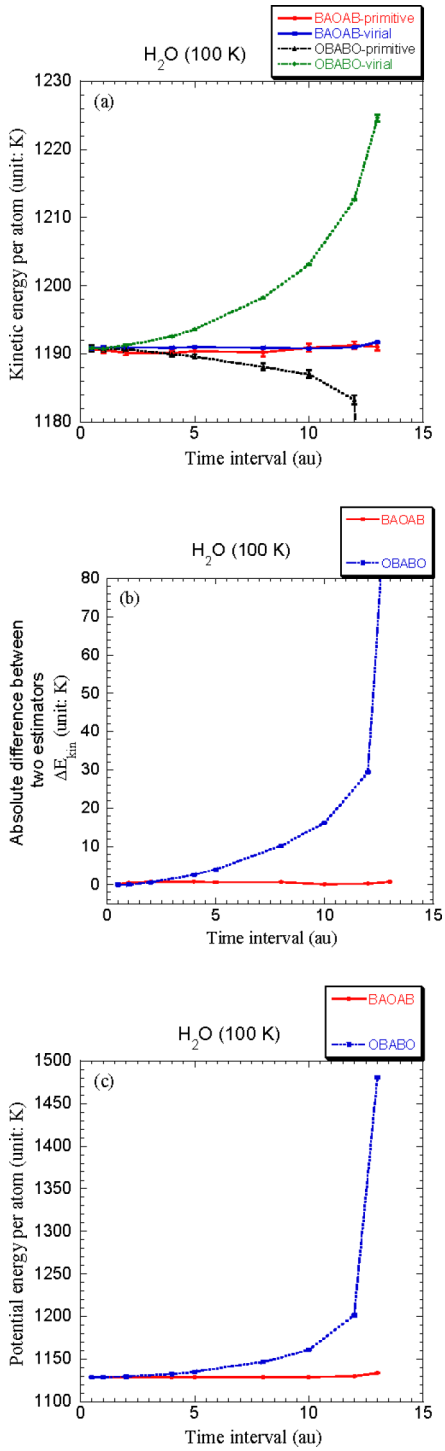

FIG. 2. As in Fig. 1, but for H_2O at T = 100 K.

125 *para*-hydrogen molecules in a box with periodic boundary conditions applied using the minimum image convention. $P = 48$ path integral beads are employed in PIMD for $T = 25$ K, while $P = 96$ for $T = 14$ K. After equilibrating the system, 16 PIMD trajectories with each propagated up to ~24.2 ns are used for estimating thermodynamic properties. While the time interval for PIMD is from ~1.2 fs to ~12.1 fs (50–500 a.u.) for $T = 25$ K, that for $T = 14$ K ranges from ~1.2 fs to ~10.2 fs (50–420 a.u.).

Figs. 3 and 4 depict comparison of the performance of OBABO to that of BAOAB for simulating liquid *para*-hydrogen at $T = 25$ K and $T = 14$ K, respectively. As shown in Figs. 3(a) and 3(b) for $T = 25$ K, while the difference between the primitive and virial estimators ΔE_{kin} of OBABO is ~0.25 K for $\Delta t = 200$ a.u. and ~1.6 K for $\Delta t = 450$ a.u., that of BAOAB is only ~0.012 K and ~0.13 K, respectively. Even

when OBABO fails at Δt = 500 a.u., BAOAB still leads to only ~0.18 K for the difference ΔE_{kin}. Similarly, as presented from Figs. 4(a) and 4(b) for T = 14 K, while the difference ΔE_{kin} for OBABO is ~0.11 K for Δt = 100 a.u. and ~1.7 K for Δt = 370 a.u., that for BAOAB is less than 0.01 K and ~0.09 K, respectively. OBABO fails when the time interval is larger than 390 a.u., however, BAOAB still produces ~0.11 K for the difference ΔE_{kin} for Δt = 420 a.u. Even when the time interval of BAOAB is 4–6 times of that of OBABO, the two PIMD integrators lead to comparable accuracy. This is also suggested by Figs. 3(c) and 4(c) where the average potential energy per molecule $\langle V(\hat{\mathbf{x}})\rangle / (N_{\mathrm{mol}} k_B)$ is examined.

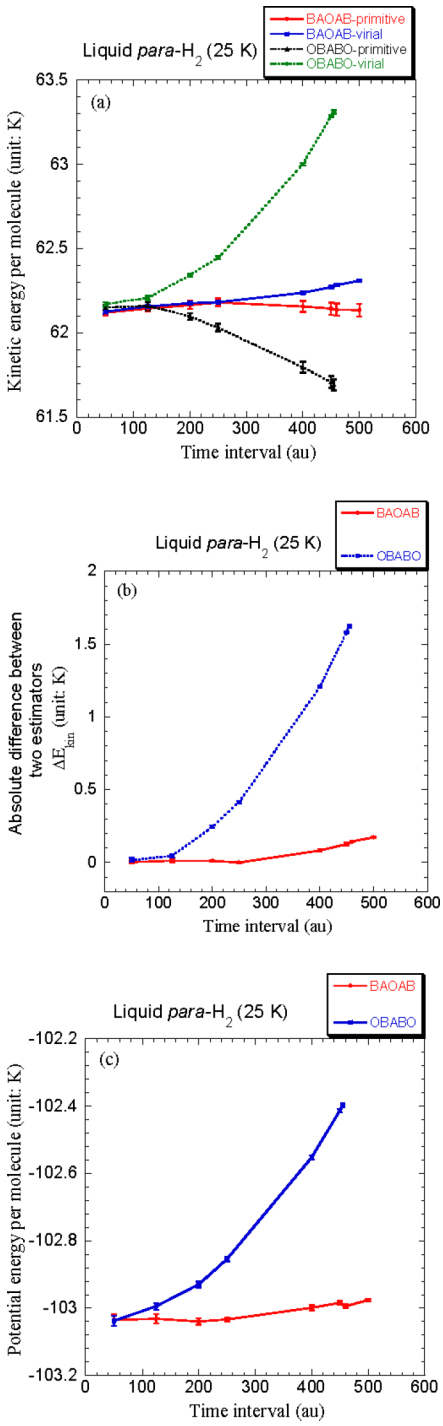

FIG. 3. PIMD results using different time intervals for liquid *para*-hydrogen at T = 25 K. (a) The average kinetic energy per molecule $\langle \hat{\mathbf{p}}^T \mathbf{M}^{-1} \hat{\mathbf{p}} \rangle / (2N_{\mathrm{mol}} k_B)$ (unit: Kelvin). Both primitive and virial estimators are used. (b) Difference between the primitive and virial estimators. (unit: Kelvin). (c) The average potential energy per molecule $\langle V(\hat{\mathbf{x}})\rangle / (N_{\mathrm{mol}} k_B)$ (unit: Kelvin). Solid line: BAOAB results. Dotted line: OBABO results. The unit of the time interval is atomic unit (a.u.). Statistical error bars are included.

C. Liquid water

For the simulation of liquid water, we employ the TTM3-F—the *ab initio* based flexible, polarizable Thole-type model for water clusters and liquid water of Fanourgakis

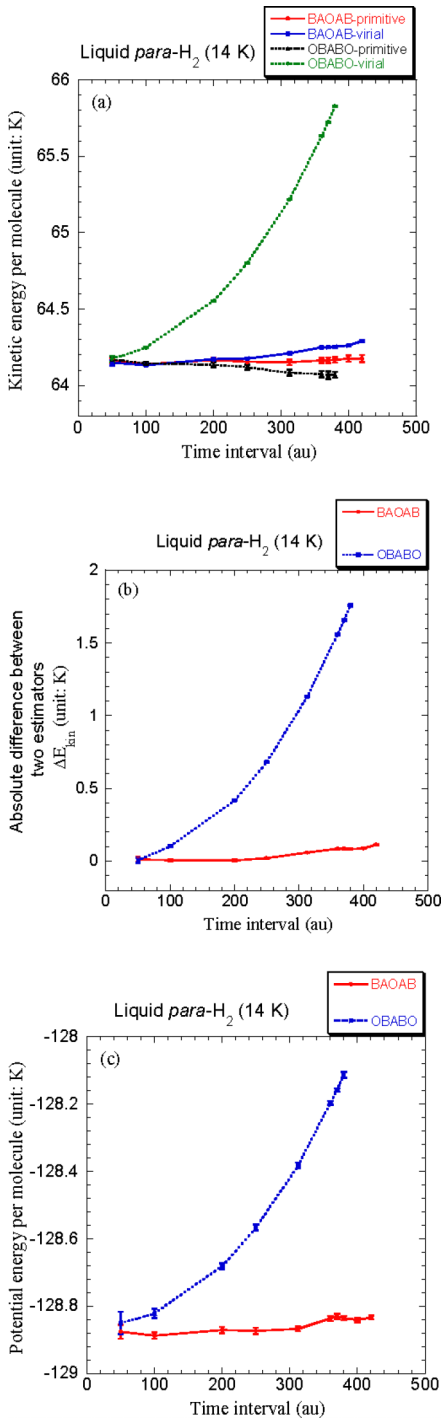

FIG. 4. As in Fig. 3, but for liquid *para*-hydrogen at T = 14 K.

and Xantheas.[32] It approximates the Born-Oppenheimer potential energy surface based on the parameterization which reproduces the binding energies and harmonic vibrational spectra of small water clusters up to $(H_2O)_{20}$ given by the second order Møller-Plesset (MP2) electronic structure theory. The TTM3-F model is able to produce good results for static equilibrium structural properties of liquid water with PIMD simulations.[32] PIMD simulations are carried out at $T = 300$ K with the liquid density $\rho_l = 0.997$ g cm^{-3} for a system of 125 water molecules in a box with periodic boundary conditions applied using the minimum image convention. $P = 72$ path integral beads are employed in the simulation. After equilibrating the system, 16 PIMD trajectories with each propagated up to ~50 ps are used for estimating thermodynamic properties. The time interval for PIMD is from 0.05 fs to 0.8 fs.

As presented in Fig. 5(a), when the time interval is $\Delta t = 0.05$ fs, both BAOAB and OBABO lead to the converged result for either the primitive or the virial estimators for the property $\langle \hat{\mathbf{p}}^T \mathbf{M}^{-1} \hat{\mathbf{p}} \rangle / (2N_{atom} k_B)$. The difference ΔE_{kin} between the results of the primitive and virial estimators is nearly zero for $\Delta t = 0.05$ fs. While the difference ΔE_{kin} for the BAOAB integrator is only ~1.7 K for $\Delta t = 0.6$ fs, that for the OBABO is ~2.5 K for $\Delta t = 0.15$ fs and ~34 K for $\Delta t = 0.6$ fs. As the time interval increases, OBABO produces ~50 K for the difference ΔE_{kin} for $\Delta t = 0.7$ fs and fails for $\Delta t = 0.8$ fs. For comparison, the BAOAB result is only ~5 K for $\Delta t = 0.8$ fs. Fig. 5(b) demonstrates that the average potential energy per atom $\langle V(\hat{\mathbf{x}}) \rangle / (N_{atom} k_B)$ obtained by BAOAB agrees well with that by OBABO within the statistical error bar for the time interval $\Delta t = 0.05$ fs, which can be considered as the converged result. While the deviation from the converged result is ~6.5 K for $\Delta t = 0.15$ fs and ~53 K for $\Delta t = 0.6$ fs for the OBABO integrator, the BAOAB result for $\Delta t = 0.6$ fs is still close to the converged result (within the statistical error bar). Even when OBABO leads to ~90 K for the deviation (from the converged result) for $\Delta t = 0.7$ fs and fails for $\Delta t = 0.8$ fs, BAOAB produces only ~11 K for the deviation (from the converged result) for $\Delta t = 0.8$ fs. In summary, the time interval can be increased by a factor of 4–6 in BAOAB for achieving the same accuracy as OBABO does.

Interestingly, in terms of accuracy as a function of the time interval, the primitive estimator Eq. (7) behaves consistently better than the virial one Eq. (8) when P is fixed for almost all the cases (Figs. 1-5(a)) studied in the present paper. As shown in Fig. 4(a) for liquid *para*-hydrogen at $T = 14$ K, the absolute value of the deviation from the converged result for the primitive estimator at $\Delta t = 380$ a.u. is only ~0.08 K for OBABO and ~0.03 K for BAOAB. For comparison, that for the virial estimator is as large as ~1.3 K for OBABO and ~0.14 K for BAOAB. Fig. 5(a) for liquid water at $T = 300$ K demonstrates that the absolute deviation for the primitive estimator at $\Delta t = 0.6$ fs is ~13 K for OBABO and ~0.3 K for BAOAB, while that for the virial estimator is as large as ~20 K for OBABO and ~1.3 K for BAOAB. Although the statistical error bar of the primitive estimator is about an order of magnitude larger than that of the virial estimator, the primitive estimator leads to more accurate results as the time interval Δt of PIMD increases.

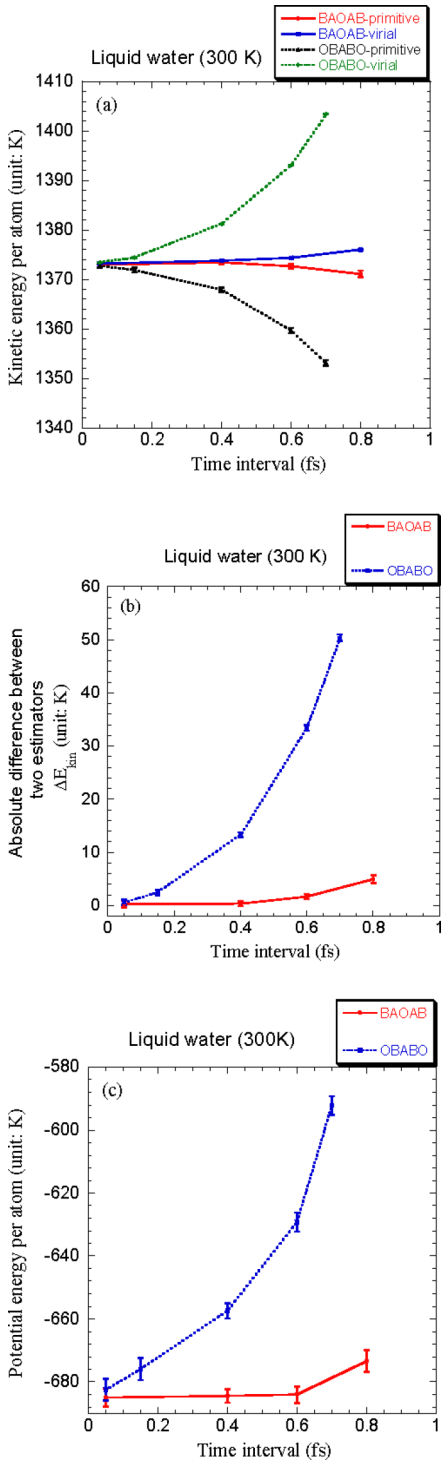

FIG. 5. PIMD results using different time intervals for liquid water at T = 300 K. (a) The average kinetic energy per atom $\langle \hat{\mathbf{p}}^T \mathbf{M}^{-1} \hat{\mathbf{p}} \rangle / (2N_{atom} k_B)$ (unit: Kelvin). Both primitive and virial estimators are used. (b) Difference between the primitive and virial estimators. (unit: Kelvin). (c) The average potential energy per atom $\langle V(\hat{\mathbf{x}}) \rangle / (N_{atom} k_B)$ (unit: Kelvin). Solid line: BAOAB results. Dotted line: OBABO results. The unit of the time interval is femtosecond (fs). Statistical error bars are included.

IV. CONCLUDING REMARKS

In this paper, we present a novel, simple, and accurate algorithm for implementing PIMD with the (white noise) Langevin thermostat. Its applications to the H_2O molecule, liquid *para*-hydrogen, and liquid water demonstrate that the

BAOAB integrator for PIMD performs uniformly better than the OBABO integrator (or equivalently PILE) for configurational sampling and for calculating thermodynamic properties. Comparing to OBABO, the BAOAB integrator reduces the error by about an order of magnitude for the same time interval of PIMD or increases the time interval by a factor of 4–6 or more for achieving the same convergence. Interestingly, an alternative approach to BAOAB (i.e., the BAOAB-num algorithm) can *further* improve the accuracy (see Appendices B and C). Although the staging transformation of path integral beads is used in PIMD for the numerical tests, the performance of BAOAB should be similar when the normal-mode transformation is employed (see the supplementary material[18]).

It is straightforward to extend BAOAB/BAOAB-num to imaginary time path integral based quantum dynamics methods. In comparison to OBABO, BAOAB increases the time interval for propagating the real time trajectory by a factor of 4–6 or more for the same convergence for path integral Liouville dynamics.[21,29,33] We expect that BAOAB/BAOAB-num also performs better than OBABO (or PILE) in thermostatted ring polymer molecular dynamics,[34] centroid molecular dynamics,[35] etc.

We note that two approaches have been proposed for combining PIMD with generalized (colored noise) Langevin thermostats.[36–38] In either approaches, it is demonstrated that the number of path integral beads P can be decreased by a factor of 4–6 to obtain converged results for thermodynamic properties such as some structural properties and the centroid-virial version of the kinetic energy.[36–38] However, caution needs to be taken for designing estimators for other general thermodynamic properties (e.g., estimators for isotope fractionation as studied by Ceriotti and Markland[39]) in such approaches, because there is no guarantee that original estimators with color noise thermostats lead to correct results.[36,38–40] For comparison, such as PILE or the BAOAB algorithm with the white noise Langevin dynamics for PIMD faithfully and consistently approaches exact results for any thermodynamic properties of any molecular systems as the number of beads P increases. It will certainly be interesting in future work to exploit the BAOAB or BAOAB-num algorithm for PIMD with colored noise Langevin thermostats[36,38] to achieve more efficiency, when reasonable estimators for the specific properties of interest are available.

ACKNOWLEDGMENTS

This work was supported by the National Science Foundation of China (NSFC) Grant Nos. 21373018 and 21573007, by the Recruitment Program of Global Experts, by Specialized Research Fund for the Doctoral Program of Higher Education No. 20130001110009, and by Special Program for Applied Research on Super Computation of the NSFC-Guangdong Joint Fund (the second phase). We acknowledge the Beijing and Tianjin supercomputer centers for providing computational resources. This research also used resources of the National Energy Research Scientific Computing Center, a DOE Office of Science User Facility supported by the Office of Science of the U.S. Department of Energy under Contract No. DE-AC02-05CH11231. J. L. thanks Mark Tuckerman and Michelle Ceriotti for useful comments on the manuscript.

APPENDIX A: DERIVATION OF THE OPTIMAL FRICTION COEFFICIENT

The Langevin equation for a harmonic oscillator $V(x) = \frac{1}{2}m\omega^2x^2$ can be expressed as

$$\ddot{x} = -\omega^2 x - \gamma_{Lang}\dot{x} + \eta(t)/m, \tag{A1}$$

with

$$\begin{aligned} \langle \eta(t) \rangle &= 0, \\ \langle \eta(t)\eta(t') \rangle &= \frac{2\gamma_{Lang}m}{\beta}\delta(t-t'), \end{aligned} \tag{A2}$$

as time averages over an infinitesimal time interval.

Implementing the Laplace transform $\hat{f}(z) = L[f(t)] = \int_0^\infty e^{-zt}f(t)\,dt$ to Eq. (A1) leads to

$$\begin{aligned} \hat{x}(z) = &\frac{zx(0)}{z^2 + \gamma_{Lang}z + \omega^2} + \frac{\gamma_{Lang}x(0) + \dot{x}(0)}{z^2 + \gamma_{Lang}z + \omega^2} \\ &+ \frac{\hat{\eta}(z)/m}{z^2 + \gamma_{Lang}z + \omega^2}. \end{aligned} \tag{A3}$$

The inverse Laplace transform of Eq. (A3) then produces

$$\begin{aligned} x(t) = &x(0)\frac{z_1e^{z_1t} - z_2e^{z_2t}}{z_1 - z_2} + \left[\gamma_{Lang}x(0) + \frac{p(0)}{m}\right]\frac{e^{z_1t} - e^{z_2t}}{z_1 - z_2} \\ &+ \frac{1}{m}\int_0^t \eta(s)\frac{e^{z_1(t-s)} - e^{z_2(t-s)}}{z_1 - z_2}ds, \end{aligned} \tag{A4}$$

with

$$\begin{aligned} z_1 &= -\frac{\gamma_{Lang}}{2} + \frac{1}{2}\sqrt{\gamma_{Lang}^2 - 4\omega^2}, \\ z_2 &= -\frac{\gamma_{Lang}}{2} - \frac{1}{2}\sqrt{\gamma_{Lang}^2 - 4\omega^2}. \end{aligned} \tag{A5}$$

Because the normalized phase space probability distribution $\rho(x,p)$ generated from the Langevin equation Eq. (A1) is

$$\frac{\beta\omega}{2\pi}\exp\left[-\beta\left(\frac{p^2}{2m} + \frac{1}{2}m\omega^2x^2\right)\right], \tag{A6}$$

it is straightforward to verify

$$\begin{aligned} m^2\beta^2\omega^4\langle x^2(0)x^2(t)\rangle = 1 &- \frac{\omega^2}{\lambda^2}e^{-\gamma_{Lang}t} \\ &+ \frac{\omega^2 + 2\lambda^2 + \lambda\gamma_{Lang}}{2\lambda^2}e^{(2\lambda - \gamma_{Lang})t} \\ &+ \frac{\omega^2 + 2\lambda^2 - \lambda\gamma_{Lang}}{2\lambda^2}e^{(-2\lambda - \gamma_{Lang})t}, \end{aligned} \tag{A7}$$

with $\lambda = (z_1 - z_2)/2$. The characteristic correlation time of the potential energy autocorrelation function

$$C_{pot}(t) = \frac{\langle [V(x(t)) - \langle V(x)\rangle][V(x(0)) - \langle V(x)\rangle]\rangle}{\langle [V(x) - \langle V(x)\rangle]^2\rangle} \tag{A8}$$

can then be shown as

$$\tau_{pot} = \int_0^\infty C_{pot}(t)\,dt = \frac{1}{2}\left(\frac{1}{\gamma_{Lang}} + \frac{\gamma_{Lang}}{\omega^2}\right). \tag{A9}$$

The smaller the τ_{pot} is, the more efficiently the Langevin equation explores the potential energy surface and samples

the configuration space. When $\gamma_{Lang} = \omega$, the characteristic correlation time τ_{pot} reaches the minimum value,

$$\tau_{pot}^{\min} = \frac{1}{\omega}. \tag{A10}$$

Since $\phi = 0$ in Eq. (25) in the free particle limit, the equations of motion for the staging modes $\left(j = \overline{2,P}\right)$ are decoupled. The Langevin equation of each degree of freedom $\left(i = \overline{1,N}\right)$ of each staging mode $\left(j = \overline{2,P}\right)$ in Eq. (25) then shares the same form as Eq. (A1). This leads to Eq. (26) for the optimal Langevin friction coefficients for PIMD with the staging transformation, because only the configurational distribution of PIMD is useful.

Ceriotti *et al.* were the first to exploit an analytical knowledge of the path integral normal mode frequencies in the free particle limit for choosing the optimal friction coefficients.[17] Here the similar strategy is employed for staging PIMD.

APPENDIX B: A SIMILAR APPROACH TO BAOAB OR OBABO

Langevin dynamics Eq. (25) can also be divided into three parts in an alternative way,

$$\begin{pmatrix} \dot{\tilde{\boldsymbol{\xi}}} \\ \dot{\mathbf{p}} \end{pmatrix} = \underbrace{\begin{pmatrix} \tilde{\mathbf{M}}^{-1}\,\mathbf{p} \\ 0 \end{pmatrix}}_{A} + \underbrace{\begin{pmatrix} 0 \\ -\omega_P^2 \bar{\mathbf{M}}\tilde{\boldsymbol{\xi}} - \dfrac{\partial \phi}{\partial \tilde{\boldsymbol{\xi}}} \end{pmatrix}}_{B} + \underbrace{\begin{pmatrix} 0 \\ -\boldsymbol{\gamma}_{Lang}\mathbf{p} + \boldsymbol{\sigma}\,\tilde{\mathbf{M}}^{1/2}\boldsymbol{\eta}\,(t) \end{pmatrix}}_{O}. \tag{B1}$$

That is, the force term $-\omega_P^2 \bar{\mathbf{M}}\tilde{\boldsymbol{\xi}}$ is moved from part A to part B in Eq. (45). The analytic propagator of the harmonic part of Eq. (45) is no longer employed.

When the splitting Eq. (38) is used for Eq. (B1), we note the new integrator BAOAB-num. Similar to Section II C, such an algorithm for propagating the PIMD trajectory through a time interval Δt for Eq. (B1) is

$$\mathbf{p}_j \leftarrow \mathbf{p}_j - \frac{\partial \phi}{\partial \tilde{\boldsymbol{\xi}}_j}\frac{\Delta t}{2} - \omega_P^2 \bar{\mathbf{M}}_j \tilde{\boldsymbol{\xi}}_j \frac{\Delta t}{2} \qquad \left(j = \overline{1,P}\right), \tag{B2}$$

$$\tilde{\boldsymbol{\xi}}_j \leftarrow \tilde{\boldsymbol{\xi}}_j + \tilde{\mathbf{M}}_j^{-1}\mathbf{p}_j \frac{\Delta t}{2} \qquad \left(j = \overline{1,P}\right), \tag{B3}$$

$$\mathbf{p}_j \leftarrow \tilde{c}_1^{(j)}\mathbf{p}_j + \tilde{c}_2^{(j)}\sqrt{\frac{1}{\beta}}\left(\tilde{\mathbf{M}}_j\right)^{1/2}\boldsymbol{\eta}_j \qquad \left(j = \overline{1,P}\right), \tag{B4}$$

$$\tilde{\boldsymbol{\xi}}_j \leftarrow \tilde{\boldsymbol{\xi}}_j + \tilde{\mathbf{M}}_j^{-1}\mathbf{p}_j \frac{\Delta t}{2} \qquad \left(j = \overline{1,P}\right), \tag{B5}$$

$$\mathbf{p}_j \leftarrow \mathbf{p}_j - \frac{\partial \phi}{\partial \tilde{\boldsymbol{\xi}}_j}\frac{\Delta t}{2} - \omega_P^2 \bar{\mathbf{M}}_j \tilde{\boldsymbol{\xi}}_j \frac{\Delta t}{2} \qquad \left(j = \overline{1,P}\right). \tag{B6}$$

Here $\boldsymbol{\eta}_j$, $\tilde{c}_1^{(j)}$, and $\tilde{c}_2^{(j)}$ are defined in the same way as in BAOAB [Eqs. (39)–(43)]. Following the same procedure as shown in Eqs. (53)–(70) of Section II D, it is straightforward to verify that the configurational distribution produced by BAOAB-num is

$$\rho_{BAOAB-num}^{config}(\tilde{\boldsymbol{\xi}}) = \rho_{eq}^{config}(\tilde{\boldsymbol{\xi}})\left\{1 + \beta\omega_P^2\Delta t^2\left[O(\varepsilon)\right] + O(\omega_P^4\Delta t^4)\right\}, \tag{B7}$$

while truncating at the 0-th order of ε for the term associated with $\omega_P^2\Delta t^2$. It is further shown in Appendix C that BAOAB-num leads to the exact configurational distribution of the beads in the harmonic limit, regardless of the time interval Δt and the friction coefficients $\boldsymbol{\gamma}_{Lang}$.

Similarly, when the splitting Eq. (31) is employed for Eq. (B1), we note the new integrator OBABO-num. Such an algorithm for propagating the PIMD trajectory through a time interval Δt for Eq. (B1) is

$$\mathbf{p}_j \leftarrow c_1^{(j)}\mathbf{p}_j + c_2^{(j)}\sqrt{\frac{1}{\beta}}\left(\tilde{\mathbf{M}}_j\right)^{1/2}\boldsymbol{\eta}_j \qquad \left(j = \overline{1,P}\right), \tag{B8}$$

$$\mathbf{p}_j \leftarrow \mathbf{p}_j - \frac{\partial \phi}{\partial \tilde{\boldsymbol{\xi}}_j}\frac{\Delta t}{2} - \omega_P^2 \bar{\mathbf{M}}_j \tilde{\boldsymbol{\xi}}_j \frac{\Delta t}{2} \qquad \left(j = \overline{1,P}\right), \tag{B9}$$

$$\tilde{\boldsymbol{\xi}}_j \leftarrow \tilde{\boldsymbol{\xi}}_j + \tilde{\mathbf{M}}_j^{-1}\mathbf{p}_j \Delta t \qquad \left(j = \overline{1,P}\right), \tag{B10}$$

$$\mathbf{p}_j \leftarrow \mathbf{p}_j - \frac{\partial \phi}{\partial \tilde{\boldsymbol{\xi}}_j}\frac{\Delta t}{2} - \omega_P^2 \bar{\mathbf{M}}_j \tilde{\boldsymbol{\xi}}_j \frac{\Delta t}{2} \qquad \left(j = \overline{1,P}\right), \tag{B11}$$

$$\mathbf{p}_j \leftarrow c_1^{(j)}\mathbf{p}_j + c_2^{(j)}\sqrt{\frac{1}{\beta}}\left(\tilde{\mathbf{M}}_j\right)^{1/2}\boldsymbol{\eta}_j \qquad \left(j = \overline{1,P}\right). \tag{B12}$$

Here $\boldsymbol{\eta}_j$, $c_1^{(j)}$, and $c_2^{(j)}$ are defined in the same way as in OBABO [Eqs. (32)–(36)]. Following the same procedure as shown in Eqs. (53)–(70) of Section II D, one finds

$$\rho_{OBABO-num}^{config}(\tilde{\boldsymbol{\xi}}) = \rho_{eq}^{config}(\tilde{\boldsymbol{\xi}})\left\{1 + \beta\omega_P^2\Delta t^2\left[\frac{1}{\varepsilon^2}\left(\frac{1}{8}\tilde{\boldsymbol{\xi}}^T\bar{\mathbf{M}}\tilde{\mathbf{M}}^{-1}\bar{\mathbf{M}}\tilde{\boldsymbol{\xi}} + \bar{\bar{G}}_{-2}\right) + \left(\frac{1}{4}\tilde{\boldsymbol{\xi}}^T\bar{\mathbf{M}}\tilde{\mathbf{M}}^{-1}\frac{\partial \phi}{\partial \tilde{\boldsymbol{\xi}}} + \bar{\bar{G}}_0\right) + O(\varepsilon)\right] + O(\omega_P^4\Delta t^4)\right\}, \tag{B13}$$

while truncating at the 0-th order of ε for the term associated with $\omega_P^2\Delta t^2$. Here $\bar{\bar{G}}_{-2}$ and $\bar{\bar{G}}_0$ are two constants required for normalization. It is easy to show that Eq. (B13) for the harmonic system [Eq. (71) or Eq. (72)] becomes

$$\begin{aligned}\rho_{OBABO-num}^{config}(\tilde{\boldsymbol{\xi}}) = {} & \rho_{eq}^{config}(\tilde{\boldsymbol{\xi}}) \\ & \times \left\{1 + \beta\omega_P^2\Delta t^2\left[\frac{1}{\varepsilon^2}\left(\frac{1}{8}\tilde{\boldsymbol{\xi}}^T\bar{\mathbf{M}}\tilde{\mathbf{M}}^{-1}\bar{\mathbf{M}}\tilde{\boldsymbol{\xi}} - \frac{1}{\beta}\frac{1}{8}\mathrm{Tr}\left(\bar{\mathbf{M}}\tilde{\mathbf{M}}^{-1}\bar{\mathbf{M}}\left(\omega_P^2\bar{\mathbf{M}} + \mathbf{K}\right)^{-1}\right)\right)\right. \\ & \left. + \left(\frac{1}{4}\tilde{\boldsymbol{\xi}}^T\bar{\mathbf{M}}\tilde{\mathbf{M}}^{-1}\mathbf{K}(\tilde{\boldsymbol{\xi}} - \tilde{\boldsymbol{\xi}}_{eq}) - \frac{1}{\beta}\frac{1}{4}\mathrm{Tr}\left(\bar{\mathbf{M}}\tilde{\mathbf{M}}^{-1}\mathbf{K}\left(\omega_P^2\bar{\mathbf{M}} + \mathbf{K}\right)^{-1}\right)\right) + O\left(\varepsilon\right)\right] + O(\omega_P^4\Delta t^4)\right\}. \end{aligned} \tag{B14}$$

Appendix C further demonstrates that the analytical form of the steady state of OBABO-num in the harmonic limit can actually be obtained. It also shows that OBABO-num does *not* even produce the exact configurational distribution for the beads in the free particle limit when the time interval Δt is finite, while the other three integrators (BAOAB, BAOAB-num, and OBABO) are able to do so. Below we compare the integrators using two examples.

Consider the 1-dimemsional model potential $V(x) = 0.25x^4$. Since the potential has no harmonic term, it presents a good test to compare BAOAB-num to the other integrators. Use $P = 1024$ beads for the inverse temperature $\beta = 8$. Fig. 6 depicts the results for the average potential energy using different time intervals of PIMD, where the four integrators (BAOAB, OBABO, BAOAB-num, and OBABO-num) are compared. In agreement with the analysis in Section II D and that in Appendix C, Fig. 6 shows that BAOAB-num is the most accurate algorithm while OBABO-num is the least. Both BAOAB and BAOAB-num demonstrate a significantly better performance than OBABO and OBABO-num.

We further compare BAOAB and BAOAB-num using the H_2O molecule at $T = 300$ K. The parameters are the same as those listed in Section III A. Fig. 7 compares the BAOAB results and the BAOAB-num ones for the average potential energy per atom using different time intervals of PIMD. When Δt is smaller than 18 a.u., BAOAB-num is more accurate than BAOAB. The two integrators produce almost the same results, when Δt is close to 18 a.u. BAOAB-num is less stable than BAOAB as the time interval Δt increases in the region $\Delta t > 18$ a.u., while both BAOAB-num and BAOAB fail when Δt is greater than 20 a.u. (as shown in Fig. 7(b) where the horizontal axis represents $\log|\langle V(\hat{\mathbf{x}})\rangle / (N_{atom}k_B)|$). When P or ω_P is significantly large, it is expected that BAOAB-num is less stable as the time interval Δt is considerably large. This is because the dominate harmonic force term is analytically integrated in part A of Eq. (45), while the same term is numerically solved in part B of Eq. (B1). It is worth emphasizing that results are not converged at all in the region where BAOAB is more accurate than BAOAB-num. Fig. 6 does not even show such a region before both integrators fail. Figs. 6 and 7 suggest that BAOAB-num always demonstrates better performance in the region where BAOAB produces reasonably converged results.

Comparison of the results for the average kinetic energy also demonstrates the same trend, which is not shown here.

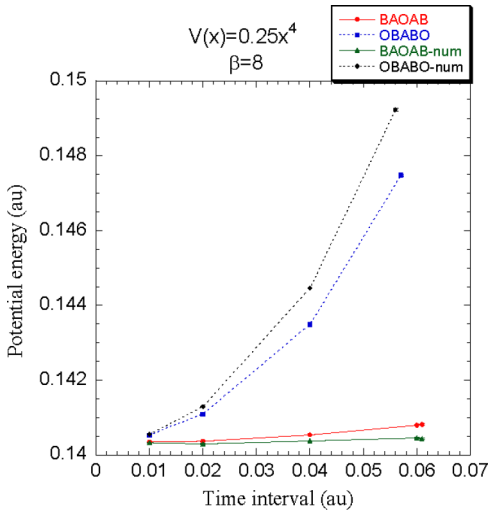

FIG. 6. PIMD results for the average potential energy $\langle V(\hat{\mathbf{x}})\rangle$ using different time intervals for $V(x) = 0.25x^4$ at $\beta = 8$. Solid line: BAOAB and BAOAB-num results. Dotted line: OBABO and OBABO-num results. The unit of either the potential energy or the time interval is atomic unit (a.u.). Statistical error bars are included.

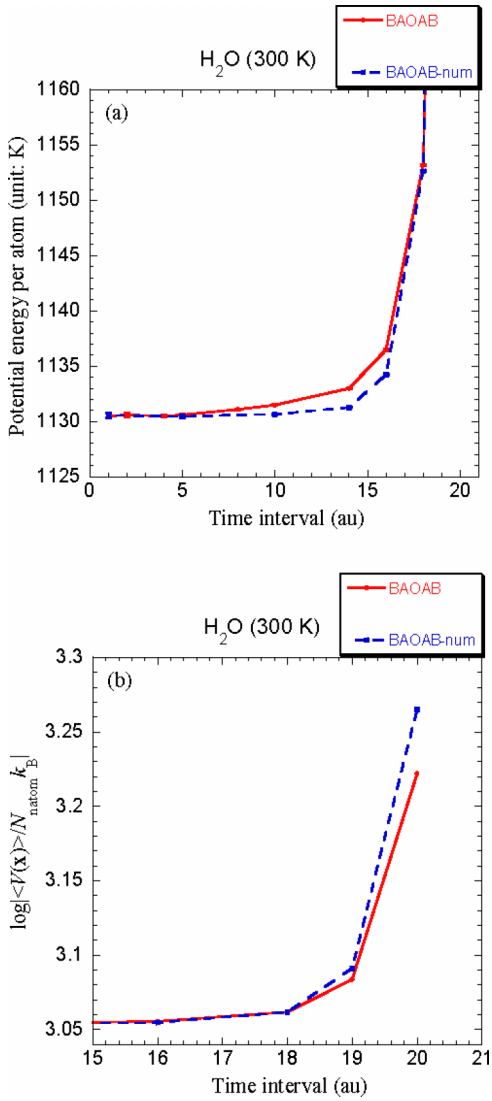

FIG. 7. PIMD results using different time intervals for H_2O at T = 300 K. (a) The average potential energy per atom $\langle V(\hat{\mathbf{x}})\rangle/(N_{atom}k_B)$ (unit: Kelvin). (b) Logarithm of the average potential energy per atom $\log|\langle V(\hat{\mathbf{x}})\rangle/(N_{atom}k_B)|$. Solid line: BAOAB results. Dashed line: BAOAB-num results. The unit of the time interval is atomic unit (a.u.). Statistical error bars are included.

APPENDIX C: ACCURACY OF THE PIMD INTEGRATOR IN THE HARMONIC LIMIT AND IN THE FREE PARTICLE LIMIT

As discussed in Section II D, while both BAOAB and OBABO are exact in the free particle limit, neither of them produces the exact configurational distribution for the path

integral beads [Eq. (69)] in the harmonic limit when the time interval Δt is finite.

Below we investigate the accuracy of BAOAB-num and that of OBABO-num proposed in Appendix B for the (general) harmonic system [Eq. (71)].

When the splitting Eq. (38) is used for Eq. (B1), the phase space propagator for BAOAB-num in the time interval Δt is

$$e^{\mathcal{L}^{BAOAB-num}\Delta t} = e^{\mathcal{L}_B^{num}\Delta t/2} e^{\mathcal{L}_A^{num}\Delta t/2} e^{\mathcal{L}_O^{num}\Delta t} e^{\mathcal{L}_A^{num}\Delta t/2} e^{\mathcal{L}_B^{num}\Delta t/2}, \tag{C1}$$

where

$$\mathcal{L}_A^{num}\rho = -\mathbf{p}^T\tilde{\mathbf{M}}^{-1}\frac{\partial\rho}{\partial\boldsymbol{\xi}}, \tag{C2}$$

$$\mathcal{L}_B^{num}\rho = \omega_P^2\boldsymbol{\xi}^T\bar{\mathbf{M}}\frac{\partial\rho}{\partial\mathbf{p}} + \left(\frac{\partial\phi}{\partial\boldsymbol{\xi}}\right)^T\frac{\partial\rho}{\partial\mathbf{p}} = \left(\frac{\partial U_{eff}}{\partial\boldsymbol{\xi}}\right)^T\frac{\partial\rho}{\partial\mathbf{p}}, \tag{C3}$$

$$\mathcal{L}_O^{num}\rho = \frac{\partial}{\partial\mathbf{p}}\cdot\left(\boldsymbol{\gamma}_{Lang}\mathbf{p}\rho\right) + \frac{1}{\beta}\frac{\partial}{\partial\mathbf{p}}\cdot\left(\boldsymbol{\gamma}_{Lang}\tilde{\mathbf{M}}\frac{\partial\rho}{\partial\mathbf{p}}\right). \tag{C4}$$

Consider the harmonic system Eq. (71), which leads to Eqs. (78) and (79). Eq. (C3) then becomes

$$\mathcal{L}_B^{num}\rho = (\boldsymbol{\xi}-\boldsymbol{\xi}_{eq})^T\boldsymbol{\Omega}\frac{\partial\rho}{\partial\mathbf{p}}. \tag{C5}$$

It is straightforward to show that the Taylor expansion $e^{\mathcal{L}_A^{num}\Delta t/2} = \sum_{n=0}^{\infty}\frac{1}{n!}\left(-\mathbf{p}^T\tilde{\mathbf{M}}^{-1}\frac{\Delta t}{2}\frac{\partial}{\partial\boldsymbol{\xi}}\right)^n$ leads to

$$e^{\mathcal{L}_A^{num}\Delta t/2} f(\boldsymbol{\xi}) = f(\boldsymbol{\xi} - \tilde{\mathbf{M}}^{-1}\mathbf{p}\frac{\Delta t}{2}). \tag{C6}$$

Similarly, one obtains

$$e^{\mathcal{L}_B^{num}\Delta t/2} g(\mathbf{p}) = g\left(\mathbf{p} + \boldsymbol{\Omega}(\boldsymbol{\xi}-\boldsymbol{\xi}_{eq})\frac{\Delta t}{2}\right). \tag{C7}$$

The OU process keeps the Maxwell momentum distribution unchanged, i.e.,

$$e^{\mathcal{L}_O^{num}\Delta t}\exp\left\{-\beta\left[\frac{1}{2}\mathbf{p}^T\tilde{\mathbf{M}}^{-1}\mathbf{p}\right]\right\} = \exp\left\{-\beta\left[\frac{1}{2}\mathbf{p}^T\tilde{\mathbf{M}}^{-1}\mathbf{p}\right]\right\}. \tag{C8}$$

Consider the density distribution

$$\rho^{BAOAB-num}(\boldsymbol{\xi},\,\mathbf{p}) = \frac{1}{Z_N}\exp\left\{-\beta\left[\frac{1}{2}\mathbf{p}^T\left(\tilde{\mathbf{M}} - \boldsymbol{\Omega}\frac{\Delta t^2}{4}\right)^{-1}\mathbf{p} + \frac{1}{2}(\boldsymbol{\xi}-\boldsymbol{\xi}_{eq})^T\boldsymbol{\Omega}(\boldsymbol{\xi}-\boldsymbol{\xi}_{eq})\right]\right\}, \tag{C9}$$

where Z_N is the normalization coefficient. Using Eqs. (C1) and (C6)–(C8), it is easy to verify

$$e^{\mathcal{L}^{BAOAB-num}\Delta t}\rho^{BAOAB-num} = \rho^{BAOAB-num}. \tag{C10}$$

That is, Eq. (C9) is a steady state of the BAOAB-num integrator. Integration over $\mathbf{p}$ in Eq. (C9) leads to

$$\begin{aligned}\rho^{config}_{BAOAB-num}(\boldsymbol{\xi}) &= \frac{1}{Z_N'}\exp\left\{-\beta\left(\frac{1}{2}(\boldsymbol{\xi}-\boldsymbol{\xi}_{eq})^T\boldsymbol{\Omega}(\boldsymbol{\xi}-\boldsymbol{\xi}_{eq})\right)\right\}\\ &= \frac{1}{Z_N'}\exp\left[-\beta U_{eff}(\boldsymbol{\xi})\right]\\ &= \rho^{config}_{eq}(\boldsymbol{\xi}),\end{aligned} \tag{C11}$$

where Z_N' is the new normalization coefficient. The BAOAB-num integrator in principle leads to the exact configurational distribution [Eq. (69)] (of the path integral beads) for the harmonic system (which includes the free particle case), irrespective of the time interval Δt (as long as the propagation Eq. (C1) is numerically stable) and the friction coefficients $\boldsymbol{\gamma}_{Lang}$.

When the number of path integral beads $P \to 1$, i.e., PIMD reduces to classical MD, BAOAB and BAOAB-num are the same in the classical limit. Eq. (C11) then suggests that the BAOAB/BAOAB-num thermostatting algorithm for classical MD leads to the *exact* classical configurational distribution for the harmonic system, regardless of the time interval Δt and the Langevin friction coefficient. Because the proof [Eqs. (C1)–(C11)] involves no approximation, this remarkable conclusion complements the analysis on BAOAB for classical MD in the large friction limit by Leimkuhler and Matthews.[26–28]

Similarly, the steady density distribution for the OBABO-num integrator for the harmonic system is

$$\rho^{OBABO-num} = \frac{1}{\bar{Z}_N}\exp\left[-\beta\left(\frac{1}{2}\mathbf{p}^T\tilde{\mathbf{M}}^{-1}\mathbf{p} + \frac{1}{2}(\boldsymbol{\xi}-\boldsymbol{\xi}_{eq})^T(\mathbf{1} - \boldsymbol{\Omega}\tilde{\mathbf{M}}^{-1}\frac{\Delta t^2}{4})\boldsymbol{\Omega}(\boldsymbol{\xi}-\boldsymbol{\xi}_{eq})\right)\right], \tag{C12}$$

which produces the configurational distribution

$$\rho^{config}_{OBABO-num} = \frac{1}{\bar{Z}_N'}\exp\left\{-\beta\left[\frac{1}{2}(\boldsymbol{\xi}-\boldsymbol{\xi}_{eq})^T\left(\mathbf{1} - \boldsymbol{\Omega}\tilde{\mathbf{M}}^{-1}\frac{\Delta t^2}{4}\right)\boldsymbol{\Omega}(\boldsymbol{\xi}-\boldsymbol{\xi}_{eq})\right]\right\}. \tag{C13}$$

Here $\bar{Z}_N$ and $\bar{Z}_N'$ are the normalization coefficients. One expands the density into a power series of Δt or $\omega_P\Delta t$ and then finds

$$\begin{aligned}\rho^{config}_{OBABO-num}(\boldsymbol{\xi}) = \rho^{config}_{eq}(\boldsymbol{\xi})&\\ \times\Bigg\{1 + \beta\omega_P^2\Delta t^2\Bigg[&\omega_P^2\left(\frac{1}{8}\boldsymbol{\xi}^T\bar{\mathbf{M}}\tilde{\mathbf{M}}^{-1}\bar{\mathbf{M}}\boldsymbol{\xi} - \frac{1}{\beta}\frac{1}{8}\mathrm{Tr}\left(\bar{\mathbf{M}}\tilde{\mathbf{M}}^{-1}\bar{\mathbf{M}}(\omega_P^2\bar{\mathbf{M}}+\mathbf{K})^{-1}\right)\right)\\ +&\left(\frac{1}{4}\boldsymbol{\xi}^T\bar{\mathbf{M}}\tilde{\mathbf{M}}^{-1}\mathbf{K}(\boldsymbol{\xi}-\boldsymbol{\xi}_{eq}) - \frac{1}{\beta}\frac{1}{4}\mathrm{Tr}\left(\bar{\mathbf{M}}\tilde{\mathbf{M}}^{-1}\mathbf{K}(\omega_P^2\bar{\mathbf{M}}+\mathbf{K})^{-1}\right)\right)\\ +&\varepsilon^2\left(\frac{1}{8}(\boldsymbol{\xi}-\boldsymbol{\xi}_{eq})^T\mathbf{K}\tilde{\mathbf{M}}^{-1}\mathbf{K}(\boldsymbol{\xi}-\boldsymbol{\xi}_{eq}) - \frac{1}{\beta}\frac{1}{8}\mathrm{Tr}\left(\mathbf{K}\tilde{\mathbf{M}}^{-1}\mathbf{K}(\omega_P^2\bar{\mathbf{M}}+\mathbf{K})^{-1}\right)\right)\Bigg] + O(\omega_P^4\Delta t^4)\Bigg\}.\end{aligned} \tag{C14}$$

While truncating at the 0-th order of ε for the term associated with $\omega_P^2\Delta t^2$, Eq. (C14) becomes

$$\rho^{config}_{OBABO-num}(\boldsymbol{\xi}) = \rho^{config}_{eq}(\boldsymbol{\xi}) \times \left\{1 + \beta\omega_P^2\Delta t^2\left[\frac{1}{\varepsilon^2}\left(\frac{1}{8}\boldsymbol{\xi}^T\bar{\mathbf{M}}\tilde{\mathbf{M}}^{-1}\bar{\mathbf{M}}\boldsymbol{\xi} - \frac{1}{\beta}\frac{1}{8}\mathrm{Tr}\left(\bar{\mathbf{M}}\tilde{\mathbf{M}}^{-1}\bar{\mathbf{M}}(\omega_P^2\bar{\mathbf{M}} + \mathbf{K})^{-1}\right)\right)\right.\right. + \left.\left.\left(\frac{1}{4}\boldsymbol{\xi}^T\bar{\mathbf{M}}\tilde{\mathbf{M}}^{-1}\mathbf{K}(\boldsymbol{\xi} - \boldsymbol{\xi}_{eq}) - \frac{1}{\beta}\frac{1}{4}\mathrm{Tr}\left(\bar{\mathbf{M}}\tilde{\mathbf{M}}^{-1}\mathbf{K}(\omega_P^2\bar{\mathbf{M}} + \mathbf{K})^{-1}\right)\right) + O(\varepsilon^2)\right] + O(\omega_P^4\Delta t^4)\right\}. \tag{C15}$$

It is consistent with Eq. (B14) except that Eq. (C15) states that the accuracy is now up to $O(\varepsilon^2)$ for the term associated with $\omega_P^2\Delta t^2$. The governing term of the error of the configurational distribution is then $\frac{\beta}{8}\boldsymbol{\xi}^T\bar{\mathbf{M}}\tilde{\mathbf{M}}^{-1}\bar{\mathbf{M}}\boldsymbol{\xi}\omega_P^4\Delta t^2$. Because ω_P is often large for converged PIMD results, comparing Eq. (C15) (or Eq. (B14)) to Eqs. (80), (82), and (C11), one finds the ascending order for the error of the configurational distribution (in the harmonic limit),

$$\mathrm{BAOAB-num} < \mathrm{BAOAB} < \mathrm{OBABO} < \mathrm{OBABO-num}. \tag{C16}$$

Finally, we consider the free particle system where $\phi = 0$. It is trivial to obtain

$$\boldsymbol{\Omega} = \omega_P^2\bar{\mathbf{M}} \tag{C17}$$

from Eq. (79). Inserting Eqs. (C17) and (77) into Eq. (C13), one obtains

$$\rho^{config}_{OBABO-num} = \frac{1}{Vol_N}\left(\frac{\beta\omega_P^2}{2\pi}\right)^{N(P-1)/2}\left|\prod_{j=2}^{P}\det\left(\bar{\mathbf{M}}_j\right)\right|^{1/2}\left|\det\left(\mathbf{1} - \omega_P^2\bar{\mathbf{M}}\tilde{\mathbf{M}}^{-1}\frac{\Delta t^2}{4}\right)\right|^{1/2} \times \exp\left\{-\beta\left[\frac{\omega_P^2}{2}\boldsymbol{\xi}^T\left(\mathbf{1} - \omega_P^2\bar{\mathbf{M}}\tilde{\mathbf{M}}^{-1}\frac{\Delta t^2}{4}\right)\bar{\mathbf{M}}\boldsymbol{\xi}\right]\right\}. \tag{C18}$$

Here $Vol_N = \int d\boldsymbol{\xi}_1 = \int d\mathbf{x}_1$ represents the volume of the system. Expanding the density into a power series of Δt or $\omega_P\Delta t$, one finds

$$\rho^{config}_{OBABO-num} = \frac{1}{Vol_N}\left(\frac{\beta\omega_P^2}{2\pi}\right)^{N(P-1)/2}\left|\prod_{j=2}^{P}\det\left(\bar{\mathbf{M}}_j\right)\right|^{1/2}\exp\left\{-\beta\left[\frac{\omega_P^2}{2}\boldsymbol{\xi}^T\bar{\mathbf{M}}\boldsymbol{\xi}\right]\right\} \times \left(1 + \beta\omega_P^2\Delta t^2\left[\frac{1}{8}\omega_P^2\boldsymbol{\xi}^T\bar{\mathbf{M}}\tilde{\mathbf{M}}^{-1}\bar{\mathbf{M}}\boldsymbol{\xi} - \frac{1}{8\beta}\mathrm{Tr}\left(\bar{\mathbf{M}}\tilde{\mathbf{M}}^{-1}\right)\right] + O\left(\omega_P^4\Delta t^4\right)\right). \tag{C19}$$

Eqs. (C13) and (C19) suggest that OBABO-num does *not* lead to the exact configurational distribution of the path integral beads even in the free particle limit, while all other three integrators (BAOAB, BAOAB-num, and OBABO) do so.

Conclusions are similar when the integrators are extended to normal mode PIMD (see the supplementary material[18]).

[1]R. P. Feynman, Phys. Rev. **91**(6), 1291–1301 (1953).
[2]D. Chandler and P. G. Wolynes, J. Chem. Phys. **74**(7), 4078–4095 (1981).
[3]D. M. Ceperley, Rev. Mod. Phys. **67**(2), 279–355 (1995).
[4]B. J. Berne and D. Thirumalai, Annu. Rev. Phys. Chem. **37**, 401–424 (1986).
[5]M. E. Tuckerman, in *Quantum Simulations of Complex Many-Body Systems: From Theory to Algorithms*, edited by J. Grotendorst, D. Marx, and A. Muramatsu (John von Neumann Institute for Computing, Jülich, 2002), Vol. 10, pp. 269–298.
[6]M. Parrinello and A. Rahman, J. Chem. Phys. **80**(2), 860–867 (1984).
[7]R. P. Feynman and A. R. Hibbs, *Quantum Mechanics and Path Integrals* (McGraw-Hill, New York, 1965).
[8]M. F. Herman, E. J. Bruskin, and B. J. Berne, J. Chem. Phys. **76**(10), 5150–5155 (1982).
[9]J. Cao and B. J. Berne, J. Chem. Phys. **99**(4), 2902–2916 (1993).
[10]M. E. Tuckerman, B. J. Berne, G. J. Martyna, and M. L. Klein, J. Chem. Phys. **99**(4), 2796–2808 (1993).
[11]M. E. Tuckerman, D. Marx, M. L. Klein, and M. Parrinello, J. Chem. Phys. **104**(14), 5579–5588 (1996).
[12]R. Hall and B. J. Berne, J. Chem. Phys. **81**(8), 3641–3643 (1984).
[13]M. J. Gillan, Phys. Rev. Lett. **58**(6), 563–566 (1987).
[14]K. Singer and W. Smith, Mol. Phys. **64**(6), 1215–1231 (1988).
[15]M. H. Müser, Comput. Phys. Commun. **147**(1-2), 83–86 (2002).
[16]A. N. Drozdov and P. Talkner, J. Chem. Phys. **109**(6), 2080–2091 (1998).
[17]M. Ceriotti, M. Parrinello, T. E. Markland, and D. E. Manolopoulos, J. Chem. Phys. **133**(12), 124104 (2010).
[18]See supplementary material at http://dx.doi.org/10.1063/1.4954990 for the case of normal mode PIMD.
[19]E. L. Pollock and D. M. Ceperley, Phys. Rev. B **30**(5), 2555–2568 (1984).
[20]J. Liu, J. Chem. Phys. **140**(22), 224107 (2014).
[21]J. Liu, D. Li, and X. Liu, Sci. Sin. Chim. **46**(1), 27–37 (2016).
[22]M. Tuckerman, B. J. Berne, and G. J. Martyna, J. Chem. Phys. **97**(3), 1990–2001 (1992).
[23]D. Janežič, M. Praprotnik, and F. Merzel, J. Chem. Phys. **122**(17), 174101 (2005).
[24]A. Ricci and G. Ciccotti, Mol. Phys. **101**(12), 1927–1931 (2003).
[25]G. Bussi and M. Parrinello, Phys. Rev. E **75**(5), 056707 (2007).
[26]B. Leimkuhler and C. Matthews, J. Chem. Phys. **138**(17), 174102 (2013).
[27]B. Leimkuhler and C. Matthews, Appl. Math. Res. Express **2013**(1), 34–56 (2013).
[28]B. Leimkuhler, C. Matthews, and G. Stoltz, IMA J. Numer. Anal. **36**(1), 13–79 (2016).
[29]J. Liu and Z. Zhang, J. Chem. Phys. **144**(3), 034307 (2016).
[30]H. Partridge and D. W. Schwenke, J. Chem. Phys. **106**(11), 4618–4639 (1997).

[31]I. F. Silvera and V. V. Goldman, J. Chem. Phys. **69**(9), 4209–4213 (1978).
[32]G. S. Fanourgakis and S. S. Xantheas, J. Chem. Phys. **128**(7), 074506 (2008).
[33]J. Liu, "An efficient algorithm for path integral Liouville dynamics" (unpublished).
[34]M. Rossi, M. Ceriotti, and D. E. Manolopoulos, J. Chem. Phys. **140**(23), 234116 (2014).
[35]J. Cao and G. A. Voth, J. Chem. Phys. **99**(12), 10070–10073 (1993).
[36]M. Ceriotti, D. E. Manolopoulos, and M. Parrinello, J. Chem. Phys. **134**(8), 084104 (2011).
[37]M. Ceriotti and D. E. Manolopoulos, Phys. Rev. Lett. **109**(10), 100604 (2012).
[38]F. Brieuc, H. Dammak, and M. Hayoun, J. Chem. Theory Comput. **12**(3), 1351–1359 (2016).
[39]M. Ceriotti and T. E. Markland, J. Chem. Phys. **138**(1), 014112 (2013).
[40]J. Shao, private communication (2016).